



**HAL**  
open science

## Growth and development of the third permanent molar in *Paranthropus robustus* from Swartkrans, South Africa

Christopher Dean, Clément Zanolli, Adeline Le Cabec, Mirriam Tawane, Jan Garrevoet, Arnaud Mazurier, Roberto Macchiarelli

### ► To cite this version:

Christopher Dean, Clément Zanolli, Adeline Le Cabec, Mirriam Tawane, Jan Garrevoet, et al.. Growth and development of the third permanent molar in *Paranthropus robustus* from Swartkrans, South Africa. *Scientific Reports*, 2020, 10 (1), pp.19053. 10.1038/s41598-020-76032-2 . hal-02987964

**HAL Id: hal-02987964**

**<https://hal.science/hal-02987964v1>**

Submitted on 4 Nov 2020


**HAL** is a multi-disciplinary open access archive for the deposit and dissemination of scientific research documents, whether they are published or not. The documents may come from teaching and research institutions in France or abroad, or from public or private research centers.

L'archive ouverte pluridisciplinaire **HAL**, est destinée au dépôt et à la diffusion de documents scientifiques de niveau recherche, publiés ou non, émanant des établissements d'enseignement et de recherche français ou étrangers, des laboratoires publics ou privés.



OPEN

# Growth and development of the third permanent molar in *Paranthropus robustus* from Swartkrans, South Africa

Christopher Dean<sup>1,2</sup>, Clément Zanolli<sup>3,4</sup>, Adeline Le Cabec<sup>3,5</sup>, Mirriam Tawane<sup>6</sup>, Jan Garrevoet<sup>7</sup>, Arnaud Mazurier<sup>8</sup> & Roberto Macchiarelli<sup>9,10</sup>

Third permanent molars (M3s) are the last tooth to form but have not been used to estimate age at dental maturation in early fossil hominins because direct histological evidence for the timing of their growth has been lacking. We investigated an isolated maxillary M3 (SK 835) from the 1.5 to 1.8-million-year-old (Mya) site of Swartkrans, South Africa, attributed to *Paranthropus robustus*. Tissue proportions of this specimen were assessed using 3D X-ray micro-tomography. Thin ground sections were used to image daily growth increments in enamel and dentine. Transmitted light microscopy and synchrotron X-ray fluorescence imaging revealed fluctuations in Ca concentration that coincide with daily growth increments. We used regional daily secretion rates and Sr marker-lines to reconstruct tooth growth along the enamel/dentine and then cementum/dentine boundaries. Cumulative growth curves for increasing enamel thickness and tooth height and age-of-attainment estimates for fractional stages of tooth formation differed from those in modern humans. These now provide additional means for assessing late maturation in early hominins. M3 formation took  $\geq 7$  years in SK 835 and completion of the roots would have occurred between 11 and 14 years of age. Estimated age at dental maturation in this fossil hominin compares well with what is known for living great apes.

The most easily observable and widely employed measure of dental maturation in modern humans, dental eruption, is in fact one of the least reliable<sup>1,2</sup>. Paradoxically, however, molar eruption has been the measure of maturation most often used in comparative studies of humans with great apes and with fossil hominins<sup>3–8</sup>. Mineralised tooth tissues (enamel and dentine), on the other hand, contain daily increments of growth that are often well-preserved, even in fossil teeth<sup>9,10</sup>. These have been used to calibrate the eruption times of first permanent molars (M1s) in fossil hominins and this has proved to be a reasonably successful method for assessing the time and patterning of dento-skeletal maturation in a broad comparative context<sup>6,11–16</sup>, if perhaps a less successful proxy for other life history variables<sup>17–20</sup>. Nonetheless, despite the fact that greater numbers of late juvenile and sub-adult fossil hominins of unknown chronological age are now associated with skeletal material approaching maturity<sup>21–28</sup>, assessing the end of the tooth maturation process remains problematic, as too few data exist to reconstruct the timing of late third permanent molar (M3) development. Indeed, to date, the age at completion of the “wisdom tooth”, i.e., the measure of late dental maturity, has never been directly reconstructed, but only inferred in australopiths (*Australopithecus* and *Paranthropus*) and early *Homo*<sup>29,30</sup>.

The initial mineralisation of the M3 tooth in both great apes and early fossil hominins occurs at a chronologically younger age than in modern humans. In *Pan* and *Gorilla*, the age range reported, albeit for relatively few individuals (Supplementary Text S1), spans almost 2.5 years, from 2.9 to 5.3 years<sup>31–37</sup>, but for a large number of modern humans the range is much greater, at least 7 years, from 5 to 12 years<sup>38–41</sup>. Radiographically, in great apes, either a large empty crypt in the jaw bone, or a minute mineralising M3 cusp tip within a crypt, appears close

<sup>1</sup>Department of Earth Sciences, Natural History Museum, London, UK. <sup>2</sup>Department of Cell and Developmental Biology, University College London, London, UK. <sup>3</sup>Univ. Bordeaux, CNRS, MCC, PACEA, UMR 5199, 33600 Pessac, France. <sup>4</sup>Department of Maxillofacial and Oral Surgery, Sefako Makgatho Health Sciences University, Ga-Rankuwa, Pretoria, South Africa. <sup>5</sup>Department of Human Evolution, Max Planck Institute for Evolutionary Anthropology, Leipzig, Germany. <sup>6</sup>Ditsong National Museum of Natural History, Pretoria, South Africa. <sup>7</sup>Deutsches Elektronen-Synchrotron DESY, Hamburg, Germany. <sup>8</sup>IC2MP, UMR 7285 CNRS, Université de Poitiers, Poitiers, France. <sup>9</sup>UMR 7194 CNRS, Muséum National D'Histoire Naturelle, Musée de L'Homme, Paris, France. <sup>10</sup>Unité de Formation Géosciences, Université de Poitiers, Poitiers, France. ✉email: ucgacrd@ucl.ac.uk

to the time of true M3 initiation. This happens as the premolars and second permanent molars (M2s) complete enamel formation (between the radiographically-defined fractional stages of tooth Crown  $\frac{3}{4}$  complete and Root initiation) and as the first permanent molars (M1s) are close to root completion (between radiographic stages Root  $\frac{3}{4}$  formed and Apex  $\frac{1}{2}$  closed) (Supplementary Table S1, Supplementary Figs. S1–S3).

Just one fossil hominin, the Early Pleistocene StW 151 from Sterkfontein, South Africa, variably attributed to early *Homo*<sup>42</sup> or *A. africanus*<sup>43</sup>, or even considered as taxonomically indeterminate<sup>16</sup>, shows evidence of a large empty M3 crypt, and is aged 4.62–4.70 years<sup>16,42</sup>. Unfortunately, the age at death of another fossil specimen with an empty M3 crypt, the Early Pleistocene early *Homo* KNM-ER 820 from Koobi Fora, Kenya<sup>44,45</sup>, is yet to be determined.

Clearly, there is insufficient evidence to determine a mean age for M3 initiation in early hominins. However, the comparative information increasingly available about the timing and sequence of these events in great apes and fossil specimens, notably for the stages of dental development both before and after M3 initiation<sup>16,37</sup>, strongly suggests M3 initiation occurred in australopiths and early *Homo* sometime between 4 and 7 years of age. Early hominin specimens aged ~4 years or less at death, such as the SK 63 *P. robustus* specimen from Swartkrans, or the *A. africanus* Taung child, both from South Africa, show no evidence of M3 initiation<sup>16,46–49</sup>. Even with a possible 3-year age range for M3 initiation, knowing the time taken for M3 crown and root formation in an early hominin would allow us to address a number of issues, including the likely age range at dental maturation.

Here we present the first histological data for the timing of M3 development in an early hominin. SK 835 is a maxillary left M3 attributed to the hominin taxon *P. robustus* and was recovered from the Early Pleistocene cave site of Swartkrans<sup>50</sup>. Following high-resolution virtual scanning and 3D imaging performed by X-ray microtomography ( $\mu$ XCT; Supplementary Fig. S4), we made thin ground sections through the crown and roots that captured the whole of tooth growth (Supplementary Texts S2–S4, Supplementary Figs. S5–S7).

We used a combination of transmitted light microscopy (TLM) and synchrotron X-ray fluorescence (SXRF) to image the daily incremental growth markings in enamel and dentine. SXRF of this specimen revealed that apparently random bands of Sr enrichment were laid down in the crown and roots of this tooth during development. These, together with other prominent accentuated markings in enamel and dentine visible in TLM, were used to align the cusps and roots of SK 835 that formed at the same time. In this way we cross-matched daily incremental growth markings from different locations within the tooth and reconstructed the growth processes involved in enamel and dentine formation. One aim of this study was to shed light on the physical nature of the circadian growth increments preserved in the enamel and dentine.

There is now good evidence that circadian clocks operate in ameloblasts and odontoblasts<sup>51–54</sup> and that they regulate amelogenin secretion and other ameloblast activities<sup>55</sup> as enamel prism formation cycles through alternating fast and slow phases<sup>56–61</sup>. How exactly this circadian rhythm manifests as a fine dark cross striation across the narrow slowly formed constriction of a prism body is however less clear<sup>55,56</sup>. Cross striations are more porous<sup>62</sup> and show a compositional contrast in back-scattered electrons-based (BSE) microscopic images that has been attributed to increased carbonate content<sup>56</sup>, or perhaps to an alternating dominance of matrix over mineral deposition during the day<sup>55</sup>. It is also likely that abrupt changes in enamel crystallite orientation and/or continuity contribute to the appearance of cross striations in TLM and in polarised light microscopy (PLM)<sup>63,64</sup>. Raman microscopy has previously shown that the peak intensity of OH, Ca<sup>2+</sup> and PO<sup>4-</sup> occurs at the prism varicosity and that the intensity of all three ions co-vary in a cyclic manner<sup>65</sup>.

Daily incremental markings in enamel and dentine enable the rates and timing of crown and root formation to be retrieved from fossil teeth. A second aim of this study was thus to quantify the changing daily rates of enamel and dentine secretion throughout the entire growth of the SK 835 early hominin M3. A further aim was to put a time scale to the fractional stages of tooth formation commonly used in comparative radiographic and other imaging studies of modern humans, great apes and fossil hominins<sup>28,37,38,66,67</sup>. Since tooth growth is a continuous and seamless process, we also reconstructed growth curves describing cuspal enamel secretion and the increase in tooth length along the once developmental boundaries between tissues, the enamel–dentine junction (EDJ) and the cementum–dentine junction (CDJ), and compared these with similar data for living hominids and fossil hominins.

## Results

**The nature of daily incremental markings.** Two regions of SK 835 that in TLM showed clear daily enamel cross striations and daily dentine increments, were scanned with SXRF (at 0.25  $\mu$ m resolution). In both tissues, the alternating light and dark increments visible in TLM corresponded most strongly with fluctuations in Ca concentration (Figs. 1 and 2). This suggests the brighter increments seen in TLM are relatively mineral dense and the darker increments less dense, which is consistent with previous BSE-based findings<sup>56,62</sup>. Broader irregular accentuated markings were also associated with more diffuse shifts in Ca concentration that spanned the underlying daily rhythms (Figs. 1 and 2). The regular daily changes in Ca concentration do not, however, occur abruptly at cross striations in the SXRF scans but more closely resemble the circadian fluctuations reported<sup>68</sup> for plasma ionized Ca<sup>2+</sup>. Interestingly in this SXRF study, unlike previous studies<sup>65</sup>, there was no discernible variation in phosphorus concentration (a major component of hydroxyapatite) where the circadian rhythm has been reported to peak twice in a day<sup>68</sup>.

**Rates of enamel formation.** Four prism tracks were defined in the first-formed cuspal enamel of the SK 835 crown (Supplementary Fig. S7). Cumulative counts of daily increments were made at 100  $\mu$ m intervals through the whole thickness of enamel, as well as measurements of cross striation spacings within ten successively formed 60-day zones of cuspal enamel formation (Supplementary Text S3, Supplementary Figs. S7–S11). Some surface enamel was lost through wear, but 575–580 daily increments are still preserved in the tallest pro-

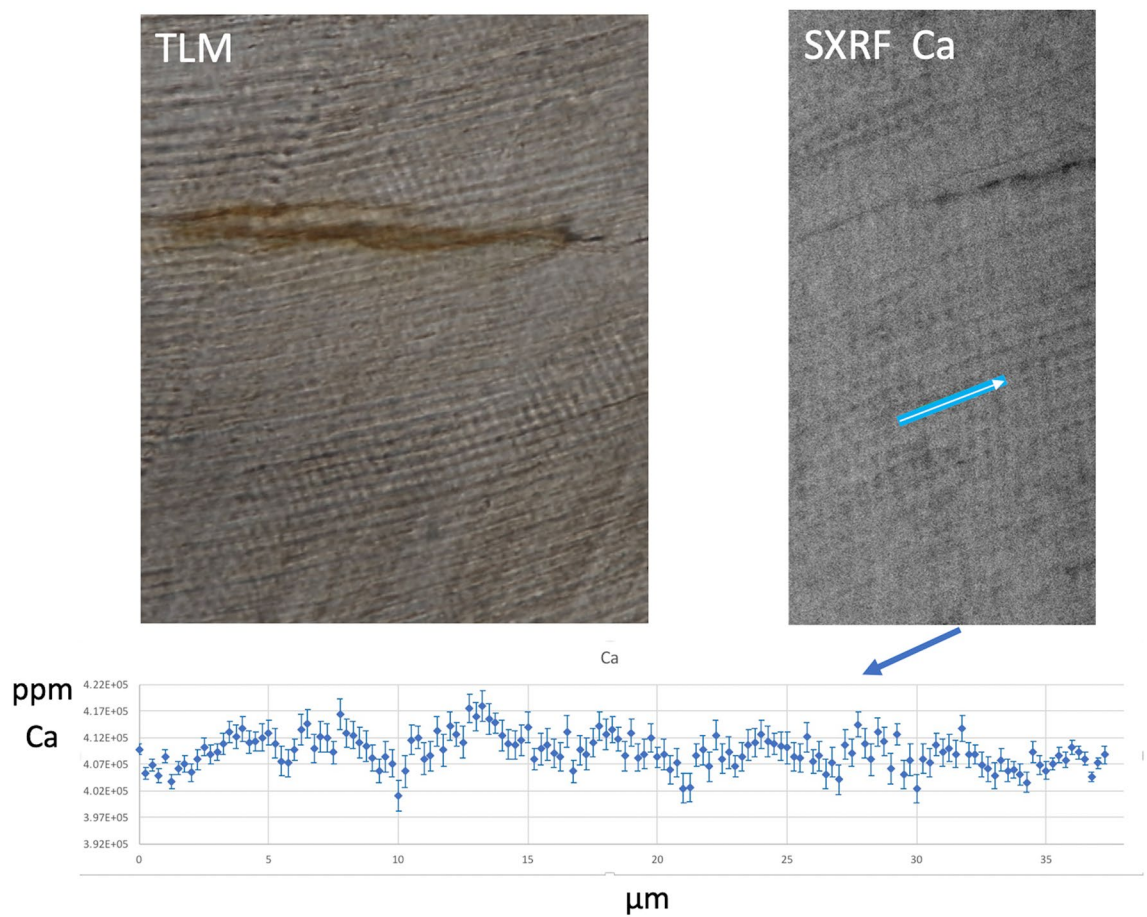


**Figure 1.** Transmitted light micrograph (TLM) of cervical enamel in the SK 835 protocone showing a region with clear daily incremental markings (left image). A SXRF (*synchrotron X-ray fluorescence*) image in the same general region showing periodic fluctuations in Ca concentration. The plot across the blue transect is ~35  $\mu\text{m}$  long and shows ~7 peaks and troughs (from left to right) in Ca concentration that fluctuate between 402,000 and 417,000 ppm. Error bars associated with each datapoint represent SD. The blue line represents the scan transect. ( $200 \times 100 \mu\text{m}^2$ , 17.0 keV, 0.25  $\mu\text{m}$ , 10 ms, scan time 1 h).

tocone cusp of this *P. robustus* M3. Formation rates ranged between 3.2  $\mu\text{m}/\text{day}$ , close to the EDJ, and rose to 8.28  $\mu\text{m}/\text{day}$  before reducing again to ~7.3  $\mu\text{m}/\text{day}$  close to the enamel surface. Formation rates in modern human molars rarely exceed 6.5  $\mu\text{m}/\text{day}$  in outer cuspal enamel, but can also take 600–700 days to form thick molar cuspal enamel, as was likely the case in SK 835 (Supplementary Figs. S8–S11). The gradient of enamel formation through the cusps of this upper M3 are greater than measured in a sample of modern human molars (Fig. 3), but similar to that in some living great apes and other early hominin molars<sup>69–71</sup>.

By combining the four trajectories of the defined prism tracks, the average time (Y) taken to form a given thickness of occlusal enamel (X) in the SK 835 *P. robustus* tooth can be predicted from the equation (Eq. 1) given here (see Supplementary Text S3 for 95% confidence intervals):

$$Y = 12.651 + .284X - 3.459e^{-5}X^2 (R^2 = .979). \quad (1)$$

**Growth in tooth length.** Teeth grow in length as cohorts of secretory cells differentiate in continuity, first along the boundaries between the EDJ in the crown, then beyond this in the root between the CDJ. The rate of differentiation (the extension rate), can be reconstructed from the daily formation rate and the slope of incremental or accentuated lines that represent the former position of the ameloblast or odontoblast cell sheet<sup>72–76</sup>. To calculate the time and rate of extension in SK 835 between initial mineralisation of the tooth and completion of its root length, we used the average times taken to form an initial 200  $\mu\text{m}$  thickness of enamel (61 days) or dentine (80 days), and the orientation of incremental markings to the EDJ or CDJ, respectively (Supplementary Texts S3–S4, Supplementary Figs. S12–S14). This was possible between protocone initiation to the end of its damaged palatal root. It was also possible in the preserved part of the paracone and separately in the detached distobuccal root (Fig. 5, Supplementary Text S4, Supplementary Fig. S7). Since each of these preserved components contain an intense SXRF Sr marker-line (Fig. 5), that formed at 4.1 years into tooth formation, they could be cross-matched in time and the cumulative tooth length plotted against formation time (Fig. 4).

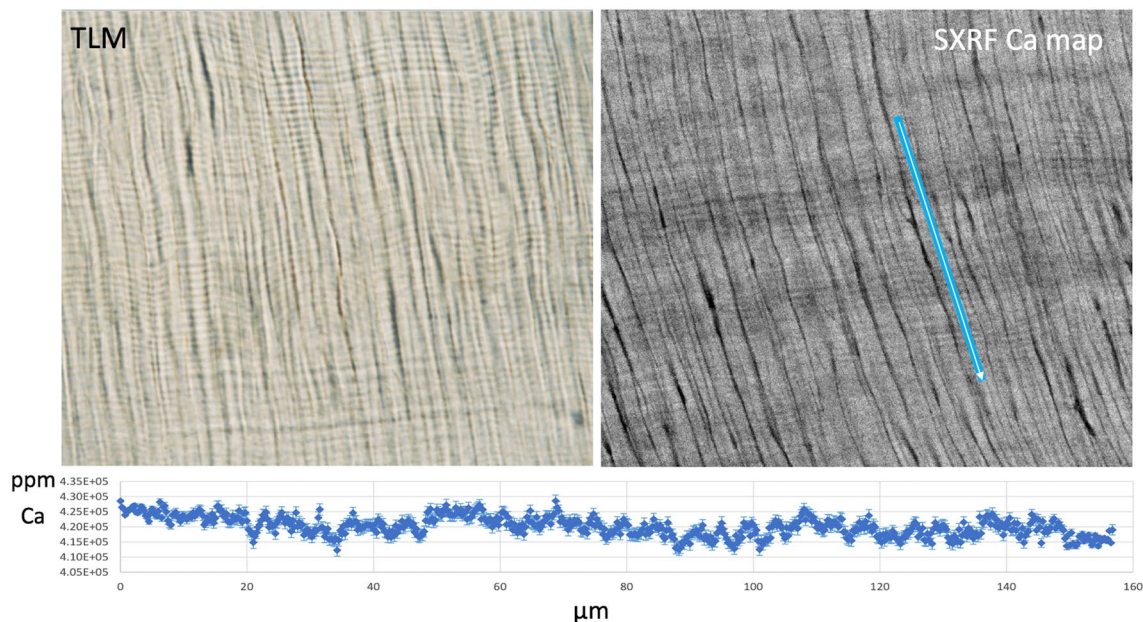


**Figure 2.** Transmitted light micrograph (TLM) of daily dentine increments in the apical root dentine of the palatal root of SK 835 (left image). A SXRF image of Ca concentration of the dentine in the same general region. The blue line is ~160 μm long and shows the transect represented in the plot of Ca concentration (from top to bottom) against distance (μm). Error bars associated with each datapoint represent SD. Across more than 30 incremental markings, Ca concentration fluctuated between 410,000 and 430,000 ppm but broader zones of lower Ca concentration spanned daily increments in some regions. (300 × 300 μm<sup>2</sup>, 17.0 keV, 0.25 μm, 10 ms, scan time 4.5 h).

For any given length (X) along the EDJ/CDJ, formation time (Y) in this *P. robustus* maxillary M3 can be predicted from the equation (Eq. 2) given here:

$$Y = .018 + 8.875e^{-5}X + 4.414e^{-8}X^2 - 3.009e^{-12}X^3 + 4.581e^{-17}X^4 + 6.494e^{-22}X^5 \quad (R^2 = .993). \quad (2)$$

**Fractional stages of tooth growth.** For modern humans and many non-human primates, defined fractions of tooth formation in cross-sectional studies have proved a more practical way of compiling chronological growth standards than longitudinal growth curves for each tooth type<sup>1,2,37,66,67</sup>. However, they remain just snapshots of a continuous and seamless growth process.

Rates of tooth growth in early hominins differ from those compiled for modern humans and so the age standards for the fractional stages defined for modern humans do not compare<sup>77–79</sup>. To reconstruct the most commonly used fractional stages of increasing tooth length (quarters of crown height and quarters of root length) for SK 835, we used the pattern of Sr banding and the accentuated markings in enamel and dentine together with the time scale derived from daily incremental markings. Figure 5 summarises the key formation times of each component in this fossil M3. In addition, we reconstructed new stages of tooth formation that represent the amount of tooth formed in quarters of crown and root formation time (Fig. 6; Supplementary Fig. S15). The last stage of root formation represented in Fig. 6 is root length completed (RC), that was attained in SK 835 at 6.67 years into M3 formation. The equation for cumulative increase in EDJ/CDJ length also allows M3 formation time in SK 835 to be predicted for any given length (Supplementary Table S2).

Using the evidence for root apex closure in SK 835 derived from its shorter mesiobuccal root to reconstruct final completion in the longer and last formed root apices, which are damaged, is problematic, but a reasonable estimate is that this may have taken a year, or so, to close (Supplementary Text S4). A safe conclusion is that the whole of M3 formation in SK 835, from the dentine horn in the crown to root apex closure, would have taken no less than 7 years, and possibly longer.

## Discussion

The estimate of ≥ 7 years for the time taken to grow an M3 in a representative of *P. robustus*, based on the data collected from the upper third molar specimen SK 835 from the 1.5–1.8 Mya site of Swartkrans, South Africa, represents the first direct evidence of this kind for any early hominin. Given a likely 4–7-year age range for M3 initiation, it now becomes possible to say that completion of the permanent dentition and root apex closure in SK 835 would have occurred sometime between 11 and 14 years of age. This estimate appears to compare well with what is known for dental maturation in living great apes<sup>19,32,34,37,80–82</sup>.

With respect to somatic growth, it has been suggested *P. robustus* showed a gorilla-like pattern of extended male growth (bimaturism)<sup>83</sup>. By assuming that, in principle, among samples of early hominins larger specimens

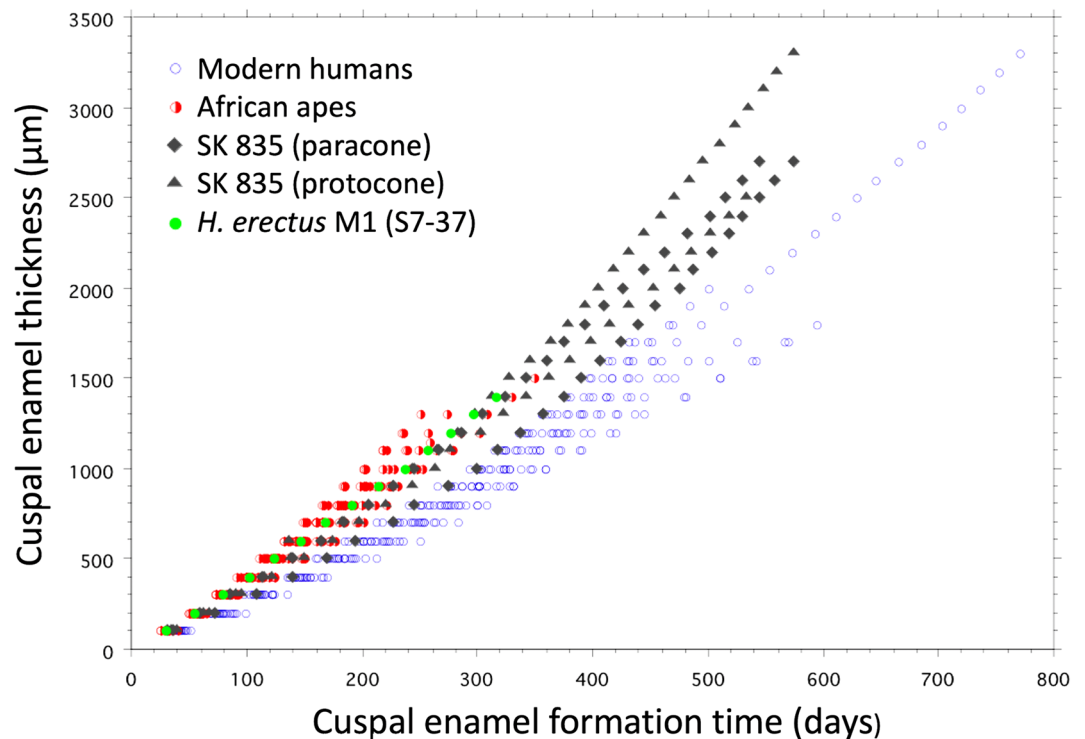


**Figure 3.** Plot showing increase of enamel thickness against enamel formation time (days). For each 100- $\mu\text{m}$  thickness of cuspal enamel, the number of daily increments were counted along prism tracks and summed. In SK 835 the trajectories between the EDJ and the enamel surface are shown as grey filled diamonds (paracone) and triangles (protocone). The lowest of these is the buccal paracone trajectory that overlaps with data for modern humans of all three molar types pooled ( $n=20$ , open blue circles). The trajectories for SK 835 are similar to a sample of African apes of all three molar types pooled ( $n=12$  *Pan*,  $n=8$  *Gorilla*, red half-filled circles) and a single M1 specimen of *H. erectus* (S7-37) (filled green circles). Thick cuspal enamel in SK 835 continues to form over a longer period of time than in African apes and early *H. erectus*. Modern human molars follow a slower trajectory. This results from slower inner rates of enamel secretion continuing at a slow rate for a longer time. Cusps may grow thick or thin along either trajectory. One human molar (M3) is exceptionally thick  $\sim 3,300$   $\mu\text{m}$  and took more than 2 years to form cuspal enamel. Daily cross striation spacings in the same human M3 are also profiled in Supplementary Fig. S10.

are more likely males and the smaller ones females<sup>84</sup>, one could argue that SK 835 more likely represents a female individual. Indeed, crown size in SK 835, especially for the mesiodistal diameter (M-D: 13.9 mm) but, to a lesser extent, also for the buccolingual diameter (B-L: 16.6 mm)<sup>50</sup>, is lower than the average values reported for the *P. robustus* upper M3s sample from Swartkrans ( $n=16$ ; M-D: 14.9 mm, range 12.7–17.2 mm; B-L: 17.0 mm, range 15.9–18.2 mm)<sup>85</sup>, and also lower, but only for the M-D diameter, than measured in the assemblage of *P. robustus* M3s from the South African sites of Swartkrans, Kromdraai and Drimolen ( $n=25$ ; M-D: 14.5 mm, range 12.1–17.2 mm; B-L: 16.5 mm, range 14.2–18.2 mm)<sup>86</sup>. Nonetheless, given the extent of tooth crown size variation, and especially of the “wisdom tooth”, this remains a hazardous exercise for all early hominins, including *P. robustus*<sup>87</sup>.

Despite the large range of daily enamel secretion rates in M3 cuspal enamel reported in this study (3.28–8.28  $\mu\text{m}/\text{day}$ ), the average cuspal rate in SK 835 (overall protocone average 5.56  $\mu\text{m}/\text{day}$ , SD=1.63; overall paracone average 4.89  $\mu\text{m}/\text{day}$ , SD=1.24) compares well with the data for KB 5223, another *Paranthropus* specimen<sup>43</sup> from the Early Pleistocene site of Kromdraai B (5.05  $\mu\text{m}/\text{day}$ ) but which has also previously been attributed to early *Homo*<sup>88</sup>. In general, these cuspal rates also compare well with the average estimates provided for *P. robustus* (5.7  $\mu\text{m}/\text{day}$ )<sup>89</sup> and with those previously determined for other fossil hominins such as StW 151 (5.53  $\mu\text{m}/\text{day}$ ) and early *Homo* (6.06  $\mu\text{m}/\text{day}$ )<sup>16</sup>. Previously published data for inner cuspal enamel formation rates in *P. robustus* (4.07–4.25  $\mu\text{m}/\text{day}$ ) have, however, tended to be higher<sup>89–91</sup> than measured in SK 835 (3.28  $\mu\text{m}/\text{day}$ ). In fact, the inner rates of occlusal enamel formation reported here for SK 835 align better with rates previously reported and summarised by Lacruz et al.<sup>71</sup> for *Pan troglodytes* (3.62  $\mu\text{m}/\text{day}$ ), *A. afarensis* (3.31  $\mu\text{m}/\text{day}$ ), *P. aethiopicus* (3.5  $\mu\text{m}/\text{day}$ ), *P. boisei* (2.94  $\mu\text{m}/\text{day}$ ), *H. rudolfensis* (3.01  $\mu\text{m}/\text{day}$ ), *H. habilis* (3.68  $\mu\text{m}/\text{day}$ ), and *H. erectus* (3.05  $\mu\text{m}/\text{day}$ ). When comparing such data sets, much depends on how close to the EDJ cross striation spacing measurements have been possible and on the different definitions of inner cuspal enamel. These new results for SK 835 do however suggest it may be premature to use summary differences in rates of enamel formation rather than gradients through time to support taxonomic differences<sup>55,92</sup>.

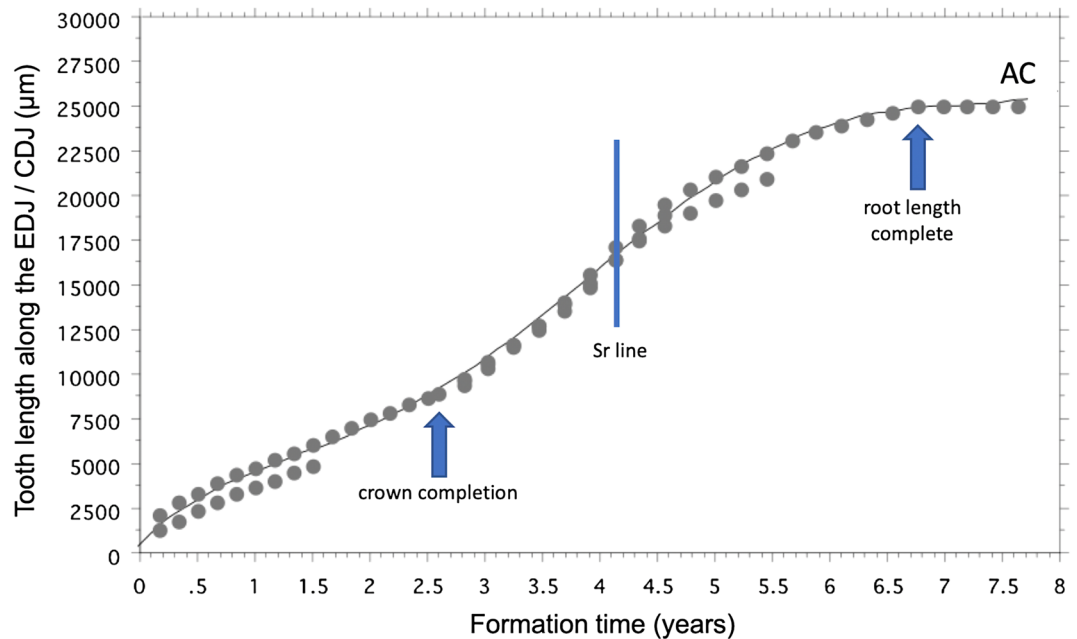


**Figure 4.** Combined plot of increase in tooth length in both cusps along the EDJ and then up to crown completion in the protocone (arrow at 2.59 years) and continuing beyond this along the CDJ in the damaged palatal root and then onwards to root length complete in the distobuccal root (arrow at 6.75 years). The roots are cross-matched at 4.12 years (Sr line). The plot is extended here to apex closure (AC) at 7.75 years. Each of the component crown and root plots are combined as a single best-fit cumulative growth curve. The plot shows increasing distance along the EDJ/CDJ ( $\mu\text{m}$ ) against formation time (years) and is expressed here by a 5th order polynomial that allows formation time (Y) to be predicted from a known value of EDJ/CDJ length (X). Although apex closure is extended to 7.75 years here, it may have taken less time. Predictions, using the following formula, of tooth formation time for each successive 1 mm of growth in length along the EDJ/CDJ are also given in Supplementary Table S2: (Eq. 2)  $Y = .018 + 8.875e^{-5}X + 4.414e^{-8}X^2 - 3.009e^{-12}X^3 + 4.581e^{-17}X^4 + 6.494e^{-22}X^5$ ;  $R^2 = .993$ .

Ramirez Rozzi<sup>79</sup> has calculated that secretory ameloblasts in thick enamelled molars attributed to *P. boisei* continue to form cuspal enamel for a greater proportion of the total crown formation time (53.8%, range in  $n = 14$  M3s, 43–73%) than, for example, in thinner enamelled gorillas (15–23%,  $n = 8$  molars). In SK 835, cuspal enamel in the protocone continued to form for 580/945 days, or 61% of the total crown formation time. Enamel thickness seems likely to be an adaptation to extend the chewing-lifespan of a tooth in the face of an abrasive diet<sup>93</sup>, but average enamel thickness (AET) is also a major component of absolute crown strength (ACS) that confers resistance to fractures associated with mechanically resistant foods<sup>94</sup>. The weaving (or decussation) of enamel prisms as they pass from the EDJ to the enamel surface is also a crack-stopping adaptation<sup>95</sup>, but strong decussation, especially close to the EDJ, is one factor that slows the rate at which cuspal enamel thickness accumulates. Prisms in *P. boisei* and *P. robustus* enamel run straighter for longer and form at a faster rate through cuspal enamel and this creates a different pattern of more tightly spaced Hunter-Schreger bands than in early *Homo* and modern humans<sup>85,96</sup>. This narrow banding pattern may be one manifestation of a trade-off to both form thick enamel resistant to a lifetime's abrasion in as short a time as possible, but which also confers maximal fracture-resistant properties with minimal decussation. However, despite *P. robustus* and modern humans both exhibiting relatively thick-enamelled molars (i.e., similar relative enamel thickness [RET] values; Supplementary Text S5, Supplementary Table S3, Supplementary Fig. S16), this condition is achieved in different ways. Molar cuspal enamel close to the EDJ in modern humans forms more slowly for a longer period of time than in *P. robustus* (Fig. 3) and other australopiths<sup>70</sup>. Cuspal enamel formation rates in *P. robustus* (SK 835) immediately start to increase from the EDJ and reach rates in the outer enamel that exceed those in modern humans (Supplementary Figs. S9–S10). Together with differences in crown shape, this relatively thick but faster-formed cuspal enamel in *P. robustus*, confers a higher crown resistance to fractures in *P. robustus* M3s than in modern humans (as assessed by the ACS index; Supplementary Table S3).

Crown formation time in SK 835 (2.59 years; Figs. 5 and 6; Supplementary Text S3) compares well with previous estimates of 2.12–2.59 years of molar crown formation times in *P. boisei* from Koobi Fora, Kenya<sup>77</sup>, and with those of 2.7 years estimated for  $n = 14$  Plio-Pleistocene hominin M3s from the Omo Valley, Ethiopia<sup>79</sup>. Both the crown formation time of SK 835 and the total tooth formation time ( $\geq 7$  years) also compare well with the only other fossil hominin molar for which the whole of tooth formation has been reconstructed histologically: the S7-37 upper M1 attributed to *H. erectus* from the Early Pleistocene site of Sangiran, Java<sup>97</sup>. In this latter specimen, crown formation took 2.6 years and total tooth formation time 7.3 years<sup>70,98,99</sup>. Figure 7 shows that the difference in growth between SK 835 and the Indonesian fossil hominin molar lies largely in the fast root extension rates

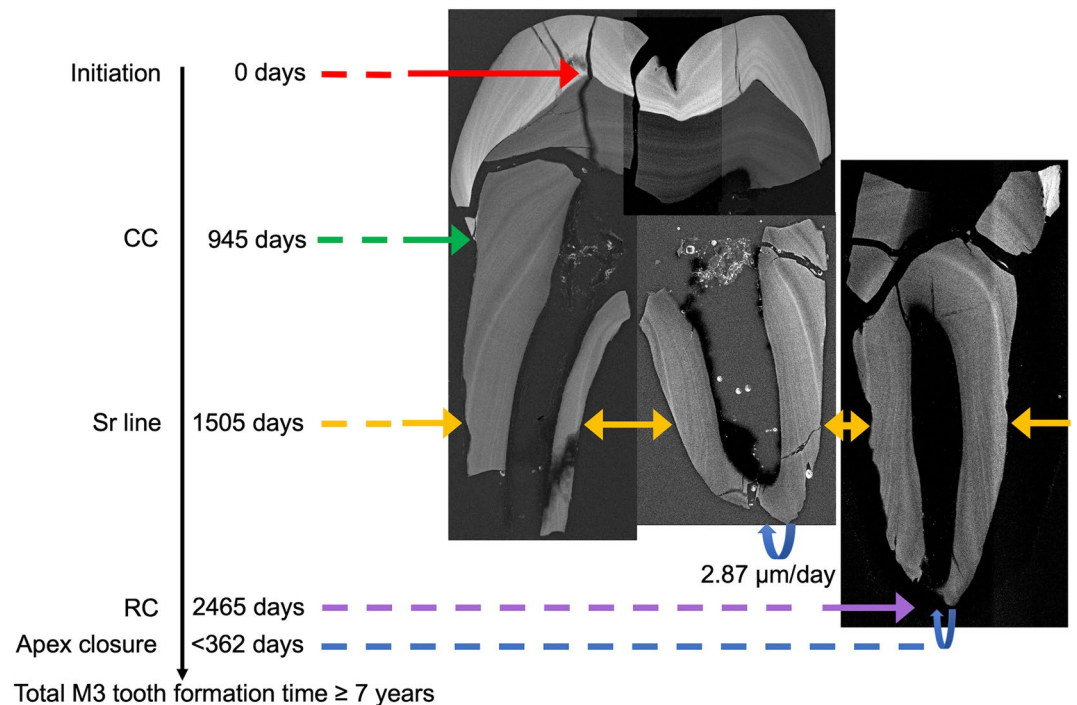


**Figure 5.** Mosaic of five SXRf montaged images showing Sr concentration (intensity) of three ground sections of SK 835. These are cross-matched to a prominent Sr line in the three separate roots (yellow arrows) that formed at 4.1 years (1505 days) into M3 formation. Tooth formation (initiation) is denoted at zero days (red arrow) in the protocone. The formation times for crown completion (945 days, green arrow) and the stage of tooth root length complete at 2465 days, (RC, purple arrow) are derived from the histological data for daily increments of growth in the crown and rates of root extension. Daily rates of dentine formation in the mesiobuccal root apex (2.87 μm/day) were used to estimate the time taken to complete closure of the distobuccal root apex (<362 days, blue dotted line). Total tooth formation time is estimated to have been ≥ 7 years.

that set the *P. robustus* tooth apart from extant humans, *Pan* and *Gorilla* as well as this single representative of *H. erectus*. Considered here in a comparative context, SK 835, with absolutely longer tooth roots, shows faster rates of root extension, and as far as can be judged from a limited sample size, most closely resembles molar tooth root growth in gorillas.

It must of course be acknowledged that these new data for M3 formation times, derived from the analysis of the *P. robustus* specimen SK 835 from Swartkrans, are for a single tooth and that the age range for M3 initiation among early hominins remains uncertain. However, they provide another line of evidence for assessing maturation during late development in fossil hominins and, importantly, one that is independent of standards established for great apes and/or modern humans<sup>1,2,37,66,67</sup>. Specifically, if the 3-year range of initiation times and stages of M3 development in SK 835 were to encompass those in other fossil hominins, they would bracket the still debated chronological age at death in TM 1517, the holotype of *P. robustus* where M3 root formation is at stage R<sub>3/4</sub><sup>28</sup>, to between 9.04 and 12.04 years. Extending these kind of age estimates to other *P. robustus* specimens with incomplete M3s seems reasonable in the absence of any other direct evidence, although age estimates for other early fossil hominins remain speculative.

Supplementary Table S4 lists some key specimens with incompletely formed M3s. For one thing it demonstrates how many early fossil hominins are known with incompletely formed M3s but for which no age at death estimates, however broad, have been possible using the M3. Based on the present results obtained for SK 835, a range of age at death estimates, all be it a wide range, is now possible when virtual histology<sup>15,16</sup> or other approaches are either impossible or impractical, or pending. Notably, the MH1 Early Pleistocene *A. sediba* from Malapa, South Africa, and another individual with a well-preserved partial skeleton attributed to *H. erectus* from West Turkana, Kenya (KNM-WT 15000), both have a complete or near-complete M3 crown<sup>14,24,30,100</sup>. Based on the findings of this study, these early hominins would both fall within the age range 6.59–9.59 years. Moreover, a further *H. erectus* specimen with associated postcranial elements from the Early Pleistocene site of Dmanisi, Georgia (D2700/D2735), with approximately half of the M3 root formed, would fall within the age range 8.26–11.26 years<sup>23,101</sup>. Based on the evidence from SK 835, it is possible to state that completion of the permanent dentition and root apex closure in early hominins generally would have been between 11 and 14 years of age.

The data presented here also allow us to re-examine previous studies of M3s in early hominins that have focused on australopith paleobiology and behaviour. Especially relevant are the contextual issues relating to australopith habitat, mobility, and growth<sup>102,103</sup>. Previous research using strontium isotope analysis suggested that *P. robustus* had a chimpanzee-like residence pattern implying male philopatry and female exogamy, i.e.,



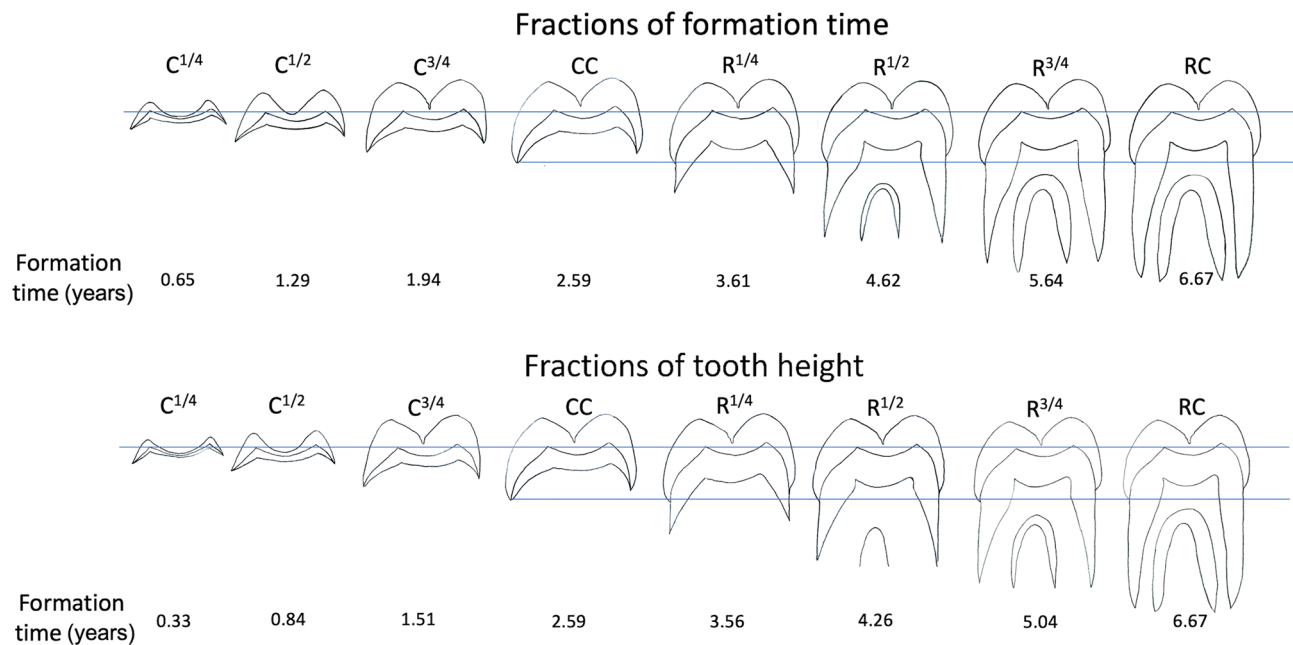


**Figure 6.** Diagrammatic representations of a *P. robustus* M3, based on SK 835, showing successive  $\frac{1}{4}$  fraction stages of time between crown initiation (Ci) and root completion (RC) as well as  $\frac{1}{4}$  fraction stages of crown height and root height. Either stages of time fractions or of height fractions can be matched to any developing hominin M3, which ever fits best, and to the formation time estimated for SK 835 (given here in years). Adding a 3-year range (from 4 to 7 years) for M3 initiation times to the age given for any fractional stage provides a range of chronological ages for dental development that, although wide, may bracket the undoubted variation there would be in M3 growth and development generally. Supplementary Table S4 lists 21 Plio-Pleistocene hominins with incomplete M3s. Note that crown completion (CC) and root completion (RC) are identical in both formation stage sequences.

with the adolescent females emigrating from their natal groups<sup>102</sup>. More recently, Sillen and Balter<sup>103</sup> measured the ratio  $^{87}\text{Sr}/^{86}\text{Sr}$  in eight M3s from Swartkrans, all attributed to *P. robustus* but of undiagnosed sex. Given that their laser ablation scan-tracks closely follow the cuspal/occlusal trajectories defined in this study, and based on our results for cuspal enamel formation times in SK 835, it can be now estimated that these laser ablation tracks are likely to span 500–600 days of enamel formed during the first half of M3 crown formation. Assuming a 3-year range for M3 initiation in *P. robustus*, this suggests that only enamel formed between ~5.5 and 8.5 years of age was sampled in all eight individuals examined by Sillen and Balter<sup>103</sup>. It is significant that all individuals showed  $^{87}\text{Sr}/^{86}\text{Sr}$  signatures consistent with having lived and died in their immediate locality at these ages, with no evidence of having moved in from elsewhere<sup>103</sup>. However, it is clear from this study that 5 or 6 years of M3 development still remained and, as Sillen and Balter<sup>103</sup> pointed out, this more than ever now leaves open questions about seasonal and/or permanent spatial displacement of *P. robustus* individuals across the differing landscapes during the later stages of M3 development. The presence of such clear Sr banding in the roots of SK 835 (Fig. 5) suggests the prospect of answering such questions is promising.

The data for M3 development presented in this study fill a gap in our knowledge about late dental development in early hominins. They provide a new and independent line of evidence for assessing the age at death of sub-adult specimens. They also demonstrate the potential of combining high-resolution elemental analysis with more traditional histological analysis of fossil tooth tissues.

## Methods

**X-ray micro-tomography ( $\mu\text{XCT}$ ).** The microtomographic acquisition of SK 835 was performed in 2015 at the PLATINA platform of the IC2MP set at the (University of Poitiers, France), with the EasyTom XL Duo laboratory device (RX-solutions, France). A sealed microfocus X-ray source (L12161-07, Hamamatsu Photonics, Japan) was used coupled to a flat panel detector (PaxScan 2520DX, Varian, USA). The specimen was scanned at a spatial resolution of 25  $\mu\text{m}$  according to the following acquisition parameters: 70 kV (tube voltage); 350  $\mu\text{A}$  (tube current); 1184 projections; 9.3 frames per second; averaging of 15 frames per projection; filtration of the beam by a 1.2 mm aluminium filter; a source-to-detector distance and a source-to-object distance of 368 mm and 72.5 mm, respectively. We applied a procedure using random shifts of the detector to avoid the presence of ring artefacts on the reconstructed images. We also recorded 32 reference images at the end of the microtomographic scan to correct for possible beam drift. The data were reconstructed in 16 bits TIF images with the XAct software (RX-solutions). For the reconstruction, we applied a filtered back projection algorithm based on the Feldkamp method for cone beam geometry associated with a Tukey filter and beam hardening artefacts were corrected through linearization with a polynomial function.

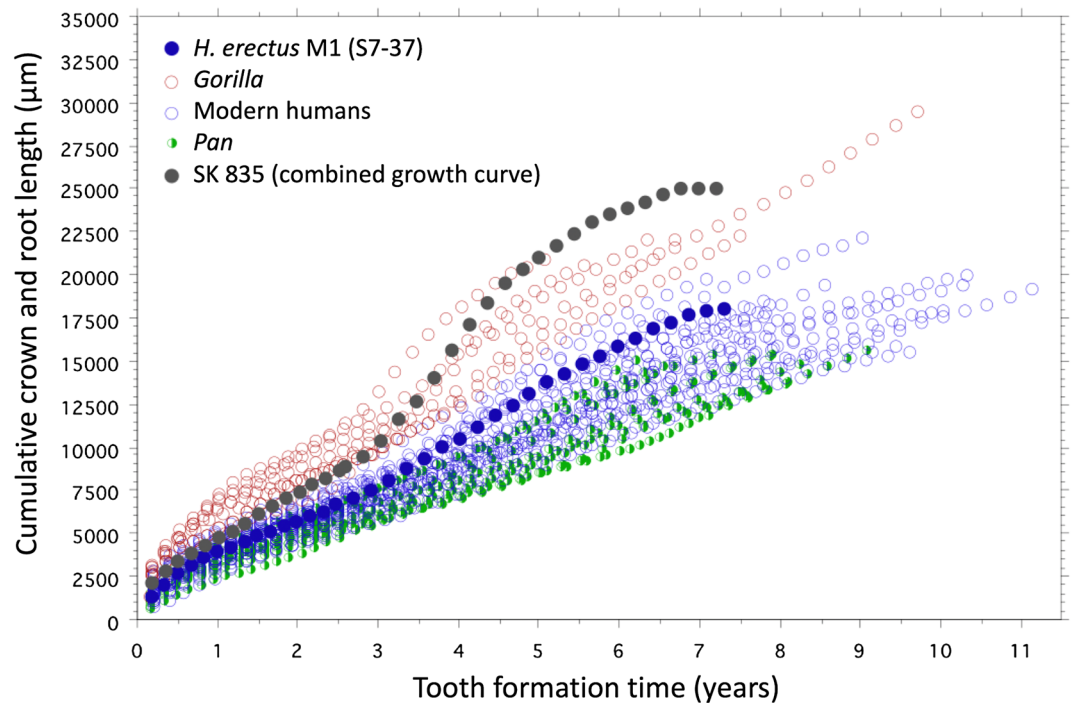


**Figure 7.** Increase in cumulative tooth length against tooth formation time. The plot shows increasing distance along the EDJ/CDJ ( $\mu\text{m}$ ) against formation time (years) for a sample of modern human molars (M2,  $n=8$ ; M3,  $n=8$ ; blue open circles), *Pan* M3s ( $n=10$ ; green half-filled circles) and *Gorilla* (M1,  $n=2$ ; M2,  $n=2$ ; M3,  $n=2$ ; red open circles), data from<sup>9,75</sup>. Superimposed onto these extant taxa are SK 835 (black filled circles) and an M1, S7-37 from Java, attributed to *H. erectus*, (dark blue filled circles), data from<sup>70,75</sup>. Increase in crown height along the EDJ in SK 835 overlaps with some modern humans and some *Gorilla* specimens. However, root growth in SK 835, that begins at 2.59 years, stands out as faster than all but a few *Gorilla* M2s and M3s. Despite having considerably longer roots than, for example the *H. erectus* M1 root, completion in these two contrasting fossil molars occurs at approximately the same time in  $\sim 7$  years from tooth initiation since rates of root extension are faster in SK 835.

**Image processing, virtual reconstruction and enamel thickness assessment.** A semiautomatic threshold-based segmentation of SK 835 was conducted using Avizo v.8.0 (FEI Visualization Sciences Group, Hillsboro), following an adaptation of the half-maximum height method<sup>104</sup>. The segmented tooth fragments were then refitted together using landmarks on corresponding aspects to reconstruct the original tooth and a constrained smoothing was applied to generate its 3D surface (Supplementary Fig. S4). Linear and surface measurements of enamel, crown dentine and pulp were taken on the virtual buccolingual section passing through the mesial dentine horns. Two bidimensional indices assessing enamel thickness were then computed based on these variables: the relative enamel thickness index (2D RET) and the absolute crown strength (ACS)<sup>94</sup>. Data for SK 835 were compared with microtomographic-based records of M3s representing *P. robustus* (original data), modern humans (original data), *Pan*<sup>105</sup> and collections of the Institut Català de Paleontologia Miquel Crusafont), *Gorilla*<sup>105</sup>, and *Pongo* (Ref.<sup>105</sup>, collections of the Institut Català de Paleontologia Miquel Crusafont, Museo di Storia Naturale di Trieste, Musée Zoologique de Strasbourg).

**Histological section preparation.** SK 835 consists of three separate crown fragments and three separate root fragments (Supplementary Text S2, Supplementary Figs. S4–S7). These were all first cleaned, scanned and imaged using  $\mu\text{XCT}$  (see above), and then either partially reassembled for sectioning or, in the case of two roots, sectioned separately. The dentine horns within the cusps were located with  $\mu\text{XCT}$  images to help define best planes of histological section. Histological methods are also provided in Dean et al.<sup>106,107</sup>. Crown and root fragments were sectioned longitudinally with a low speed diamond saw (*Buehler IsoMet*). The cut block face that contained the best plane of section was lightly lapped through a series of silicon carbide abrasive papers (*Buehler CarbiMet*, P800–P1200) and then taken to a mirror finish using  $1\ \mu\text{m}$  aluminium oxide powder (*Buehler MicroPolish*) and deionised water on a felt polishing pad (*Buehler ChemoMet*). Polishing and cutting residue was cleared from the block in an ultrasonic bath. After 24 h in a silica gel desiccator, the polished block face was fixed under pressure for 48 h to a 1 mm thick glass slide using a low viscosity slow-curing dual component epoxy resin designed for glass (*Huntsman Araldite 2020*). A second cut was then made parallel with the block face/glass slide leaving  $\sim 300\ \mu\text{m}$  tooth tissue attached to the slide. This was lapped plane-parallel to  $\sim 100\ \mu\text{m}$  in a hand-held extrudable steel slide holder (*Buehler*) first on fine wet abrasive papers (P2500) and then for final polishing on a soft polishing cloth (*Buehler MicroCloth*) with a  $1\ \mu\text{m}$  diamond suspension (*MetaDi Poly 1\ \mu\text{m}*) to ensure

no surface contamination (e.g., with alumina powder) that might affect SXRF scans. While SXRF scans were performed without a coverslip, sections were cleared in xylene and mounted with DPX (Distyrene, Phthalate plasticiser in xylene) for transmitted light microscopy.

**Synchrotron X-ray fluorescence (SXRF) imaging.** Experiments were performed on the P06 Beamline<sup>108,109</sup>, Petra III, at DESY (Deutsches Elektronen-Synchrotron, Hamburg, Germany, a member of the Helmholtz Association HGF). The storage ring was operated in 40-bunch mode using top-up filling mode with a current of 100 mA ± 0.5 mA. The primary X-ray beam was monochromatised to 17.0 keV using a double crystal Si111 monochromator and focused using a Kirkpatrick-Baez (KB) mirror system (*JTEC, Japan*) to 500 × 500 nm<sup>2</sup>. For this experiment, the set-up comprised a Maia 384C detector system<sup>110</sup>, ideally used in “back-scatter” geometry to maximise the solid angle during analysis of thin polished samples (~ 100 µm-thick in this study) and allowing for large area SXRF imaging with a sub-µm resolution using millisecond dwell times<sup>111</sup>. Further details on the set-up are provided in Dean et al.<sup>106,107</sup>. Elements of primary interest were Ca and Sr. Spectral analysis, deconvolution and initial image analysis of the fluorescence data were performed using GeoPIXE 7.4f.<sup>112</sup> The X-ray yield calculations were performed assuming a hydroxyapatite matrix (Ca<sub>10</sub>(PO<sub>4</sub>)<sub>6</sub>(OH)<sub>2</sub>) with density 3.1 g/cm<sup>3</sup> close to enamel<sup>113</sup> and final sample thickness of 80–100 µm. Glass slides were included in the overall sample model as appropriate. Concentrations were determined using a conversion factor (photon counts to equivalent charge) through measurement of a standard Ni foil with areal density 50.0 µg/cm<sup>2</sup> (*Micromatter Technologies Inc. Canada*). Elemental distribution maps were normalised to the incoming X-ray flux. SXRF concentrations are reported as parts-per-million (ppm or µg/g).

Overview scans of the mesiobuccal and distobuccal roots of SK 835 were made at 10 µm, 10 ms, and each took 5.0 h. Scans of the central cuspal/occlusal enamel, the protocone and palatal root together, and the paracone, were also performed at 10 µm, 10 ms, and took between 1.3 and 5.5 h. Two regions of interest were then scanned to image daily enamel cross striations (at 0.25 µm 10 ms and 1 h) and daily dentine increments (at 0.25 µm 10 ms and 4.5 h). Using GeoPIXE 7.4f., two sets of elemental profiles for Ca were made along transects defined on the SXRF scans of enamel and dentine daily increments (Figs. 1 and 2).

**Histological methods.** Data for daily rates of enamel and dentine formation were collected with TLM (Supplementary Texts S3–S4). Groups of ameloblasts secrete prisms (long bundles of hydroxyapatite crystallites) that extend from the EDJ to the enamel surface. The change in spacing (or repeat interval) of daily enamel cross striations along prisms was measured and counted through enamel in SK 835 to provide rates and times of cuspal enamel formation. Repeated measurements across groups of daily increments in enamel and dentine were made at multiple locations within a 200-µm zone of the EDJ or CDJ and an average value was used as the rate of formation for this given thickness of tissue. Previous methods of calculating total enamel formation times<sup>58,59,72,114</sup> were adapted to estimate the rate at which ameloblasts and odontoblasts differentiated, or extended, across the whole length of the crown and/or root<sup>73–75,115</sup>. At the start of crown or root formation, a line was projected from the EDJ or CDJ (point ‘a’ in Supplementary Fig. S14) along the direction of enamel or dentine apposition to a point 200 µm deep (point ‘c’ in Supplementary Fig. S14). Accentuated incremental markings representing the slope of the original forming cell sheet were identified at point ‘c’ and traced back to, but further along, the EDJ or CDJ in the direction of crown and root formation (point ‘b’ in Supplementary Fig. S14). The rate of increase in crown or root length (defined as the extension rate<sup>72</sup>) equals the distance between points ‘a’ and ‘b’ divided by the time taken to form the 200-µm thickness of tissue between ‘a’ and ‘c’ (Supplementary Fig. S14). This procedure was repeated consecutively to the end of tooth formation and the cumulated data plotted as a growth curve.

## Data availability

Raw images and derived data supporting the findings of this study are available from the corresponding author (C.D.) on request.

Received: 5 August 2020; Accepted: 15 October 2020

Published online: 04 November 2020

## References

- Konigsberg, L. & Holman, D. L. 11 Estimation of age at death from dental emergence and implications. In *Human Growth in the Past: Studies from Bones and Teeth* vol. 25 (eds Hoppa, R. D. & FitzGerald, C. M.) 264–289 (Cambridge University Press, Cambridge, 1999).
- Liversidge, H. M. Variation in modern human dental development. In *Growth and Development in the Genus Homo* (eds Thompson, J. L. et al.) 73–113 (Cambridge University Press, Cambridge, 2003).
- Dart, R. A. *Australopithecus africanus*: The Man-Ape of South Africa. *Nature* **115**, 195–199 (1925).
- Schultz, A. H. Eruption and decay of the permanent teeth in primates. *Am. J. Phys. Anthropol.* **19**, 489–581 (1935).
- Schultz, A. H. *The Life of Primates* (Universe Books, Bloomington, 1969).
- Smith, B. H. Dental development as a measure of life history in primates. *Evolution* **43**, 683–688 (1989).
- Smith, B. H. Life history and the evolution of human maturation. *Evol. Anthropol. Issues News Rev.* **1**, 134–142 (1992).
- Kelley, J. & Schwartz, G. T. Life-history inference in the early hominins *Australopithecus* and *Paranthropus*. *Int. J. Primatol.* **33**, 1332–1363 (2012).
- Dean, M. C. Retrieving chronological age from dental remains of early fossil hominins to reconstruct human growth in the past. *Philos. Trans. R. Soc. B Biol. Sci.* **365**, 3397–3410 (2010).
- Dean, C. How the microstructure of dentine can contribute to reconstructing developing dentitions and the lives of hominoids and hominins. *C. R. Palévol.* **16**, 557–571 (2017).
- Bromage, T. G. & Dean, M. C. Re-evaluation of the age at death of immature fossil hominids. *Nature* **317**, 525–527 (1985).
- Smith, B. H. Dental development in *Australopithecus* and early *Homo*. *Nature* **323**, 327–330 (1986).

13. Dean, M. C. Tooth microstructure tracks the pace of human life-history evolution. *Proc. R. Soc. B Biol. Sci.* **273**, 2799–2808 (2006).
14. Le Cabec, A., Tafforeau, P., Smith, T. M., Carlson, K. J. & Berger, L. R. Dental development of the *Australopithecus sediba* juvenile MH1 determined from synchrotron virtual paleohistology. In *Proceedings of the European Society for the study of Human Evolution 3* 103 (2014).
15. Le Cabec, A., Tang, N. K. & Tafforeau, P. Accessing developmental information of fossil hominin teeth using new synchrotron microtomography-based visualization techniques of dental surfaces and interfaces. *PLoS ONE* **10**, e0123019 (2015).
16. Smith, T. M. *et al.* Dental ontogeny in pliocene and early pleistocene hominins. *PLoS ONE* **10**, e0118118 (2015).
17. Robson, S. L. & Wood, B. Hominin life history: reconstruction and evolution. *J. Anat.* **212**, 394–425 (2008).
18. Smith, T. M. *et al.* First molar eruption, weaning, and life history in living wild chimpanzees. *Proc. Natl. Acad. Sci.* **110**, 2787 (2013).
19. Machanda, Z. *et al.* Dental eruption in East African wild chimpanzees. *J. Hum. Evol.* **82**, 137–144 (2015).
20. Kelley, J., Schwartz, G. T. & Smith, T. M. Age at first molar emergence in *Pan troglodytes verus* and variation in the timing of molar emergence among free-living chimpanzees. *J. Hum. Evol.* **145**, 102823 (2020).
21. Brown, F., Harris, J., Leakey, R. & Walker, A. Early *Homo erectus* skeleton from west Lake Turkana, Kenya. *Nature* **316**, 788–792 (1985).
22. Walker, A. & Leakey, R. (eds) *The Nariokotome Homo erectus Skeleton* (Harvard University Press, Cambridge, 1993).
23. Lordkipanidze, D. *et al.* Postcranial evidence from early *Homo* from Dmanisi, Georgia. *Nature* **449**, 305–310 (2007).
24. Berger, L. R. *et al.* *Australopithecus sediba*: A new species of *Homo*-like australopithec from South Africa. *Science* **328**, 195–204 (2010).
25. Berger, L. R. *et al.* *Homo naledi*, a new species of the genus *Homo* from the Dinaledi Chamber, South Africa. *eLife* **4**, e09560 (2015).
26. Cameron, N., Bogin, B., Bolter, D. & Berger, L. R. The postcranial skeletal maturation of *Australopithecus sediba*. *Am. J. Phys. Anthropol.* **163**, 633–640 (2017).
27. Bolter, D. R., Elliott, M. C., Hawks, J. & Berger, L. R. Immature remains and the first partial skeleton of a juvenile *Homo naledi*, a late Middle Pleistocene hominin from South Africa. *PLoS ONE* **15**, e0230440 (2020).
28. Cazenave, M. *et al.* Reassessment of the TM 1517 odonto-postcranial assemblage from Kromdraai B, South Africa, and the maturational pattern of *Paranthropus robustus*. *Am. J. Phys. Anthropol.* **172**, 714–722 (2020).
29. Beynon, A. D. & Dean, M. C. Distinct dental development patterns in early fossil hominids. *Nature* **335**, 509–514 (1988).
30. Dean, M. C. & Smith, B. H. Growth and development of the nariokotome youth, KNM-WT 15000. In *The First Humans—Origin and Early Evolution of the Genus Homo: Contributions from the Third Stony Brook Human Evolution Symposium and Workshop October 3rd–October 7th* (eds Grine, F. E. *et al.*) 101–120 (Springer, Dordrecht, 2009).
31. Anemone, R. L., Watts, E. S. & Swindler, D. R. Dental development of known-age chimpanzees, *Pan troglodytes* (primates, pongidae). *Am. J. Phys. Anthropol.* **86**, 229–241 (1991).
32. Anemone, R. L., Mooney, M. P. & Siegel, M. I. Longitudinal study of dental development in chimpanzees of known chronological age: implications for understanding the age at death of Plio-Pleistocene hominids. *Am. J. Phys. Anthropol.* **99**, 119–133 (1996).
33. Beynon, A. D., Dean, M. C. & Reid, D. J. Histological study on the chronology of the developing dentition in gorilla and orangutan. *Am. J. Phys. Anthropol.* **86**, 189–203 (1991).
34. Kuykendall, K. L. Dental development in chimpanzees (*Pan troglodytes*): The timing of tooth calcification stages. *Am. J. Phys. Anthropol.* **99**, 135–157 (1996).
35. Dean, C. & Wood, B. A digital radiographic atlas of great apes skull and dentition. In *Digital Archives of Human Paleobiology* (eds Bondioli, L. & Macchiarelli, R.) (ADS Solutions, Milan, 2003).
36. Schwartz, G. T., Reid, D. J., Dean, M. C. & Zihlman, A. L. A faithful record of stressful life events recorded in the dental developmental record of a juvenile gorilla. *Int. J. Primatol.* **27**, 1201–1219 (2006).
37. Kralick, A. E. *et al.* A radiographic study of permanent molar development in wild Virunga mountain gorillas of known chronological age from Rwanda. *Am. J. Phys. Anthropol.* **163**, 129–147 (2017).
38. Liversidge, H. M. Timing of human mandibular third molar formation. *Ann. Hum. Biol.* **35**, 294–321 (2008).
39. Liversidge, H. M. Predicting mandibular third molar agenesis from second molar formation. *Acta Stomatol. Croat.* **42**, 311–317 (2008).
40. AlQahtani, S. J., Hector, M. P. & Liversidge, H. M. Brief communication: the London atlas of human tooth development and eruption. *Am. J. Phys. Anthropol.* **142**, 481–490 (2010).
41. Reid, D. J. & Guatelli-Steinberg, D. Updating histological data on crown initiation and crown completion ages in southern Africans. *Am. J. Phys. Anthropol.* **162**, 817–829 (2017).
42. Moggi-Cecchi, J., Tobias, P. V. & Beynon, A. D. The mixed dentition and associated skull fragments of a juvenile fossil hominin from Sterkfontein, South Africa. *Am. J. Phys. Anthropol.* **106**, 425–465 (1998).
43. Zanolli, C. *et al.* What is South African early *Homo*? New insights from the molar endostructural signature. *Proc. Eur. Soc. Study Hum. Evol.* **7**, 206 (2018).
44. Leakey, R. E. F. & Wood, B. A. New evidence of the genus *Homo* from East Rudolf, Kenya. II. *Am. J. Phys. Anthropol.* **39**, 355–368 (1973).
45. Dean, M. C. The dental developmental status of six East African juvenile fossil hominids. *J. Hum. Evol.* **16**, 197–213 (1987).
46. Conroy, G. C. & Vannier, M. W. Dental development in South African australopithecines. Part I: Problems of pattern and chronology. *Am. J. Phys. Anthropol.* **86**, 121–136 (1991).
47. Dean, M. C., Beynon, A. D., Thackeray, J. F. & Macho, G. A. Histological reconstruction of dental development and age at death of a juvenile *Paranthropus robustus* specimen, SK 63, from Swartkrans, South Africa. *Am. J. Phys. Anthropol.* **91**, 401–419 (1993).
48. Dean, M. C. Hominoid tooth growth; using incremental lines in dentine as markers of growth in modern human and fossil primate teeth. In *Human Growth in the Past. Studies from Bones and Teeth* (eds Hoppa, R. & FitzGerald, C.) 111–127 (Cambridge University Press, Cambridge, 1999).
49. Lacruz, R. S., Ramirez Rozzi, F. V. & Bromage, T. G. Dental enamel hypoplasia, age at death, and weaning in the Taung child. *South Afr. J. Sci.* **101**, 567–569 (2005).
50. Robinson, J. T. *The Dentition of the Australopithecinae* (Transvaal Museum, Pretoria, 1956).
51. Athanassiou-Papaefthymiou, M. *et al.* Molecular and circadian controls of ameloblasts. *Eur. J. Oral Sci.* **119**, 35–40 (2011).
52. Lacruz, R. S. *et al.* The circadian clock modulates enamel development. *J. Biol. Rhythms* **27**, 237–245 (2012).
53. Zheng, L. *et al.* The tick tock of odontogenesis. *Exp. Cell Res.* **325**, 83–89 (2014).
54. Papakyrikos, A. M. *et al.* Biological clocks and incremental growth line formation in dentine. *J. Anat.* **237**, 367–378 (2020).
55. Lacruz, R. S. Chapter 4: genetic regulation of amelogenesis and implications for hominin ancestors. In *Developmental Approaches to Human Evolution* (eds Boughner, J. C. & Rolian, C.) 61–75 (Wiley, Hoboken, 2015).
56. Boyde, A. Carbonate concentration, crystal centers, core dissolution, caries, cross striations, circadian rhythms, and compositional contrast in the SEM. *J. Dent. Res.* **58**, 981–983 (1979).
57. Boyde, A. E. In *Handbook of Microscopic Anatomy* (eds Oksche, A. & Vollrath, L.) Vol. 6, 309–473 (Springer, Berlin Heidelberg, 1989).
58. Boyde, A. Developmental interpretations of dental microstructure. *Primate Life Hist. Evol. Monogr. Primatol.* **14**, 229–267 (1990).

59. Risnes, S. Enamel apposition rate and the prism periodicity in human teeth. *Eur. J. Oral Sci.* **94**, 394–404 (1986).
60. Bromage, T. G. Enamel incremental periodicity in the pig-tailed macaque: a polychrome fluorescent labeling study of dental hard tissues. *Am. J. Phys. Anthropol.* **86**, 205–214 (1991).
61. Zheng, L. *et al.* Circadian rhythms regulate amelogenesis. *Bone* **55**, 158–165 (2013).
62. Shellis, R. P. Relationship between human enamel structure and the formation of caries-like lesions in vitro. *Arch. Oral Biol.* **29**, 975–981 (1984).
63. Risnes, S. Growth tracks in dental enamel. *J. Hum. Evol.* **35**, 331–350 (1998).
64. Li, C. & Risnes, S. SEM observations of Retzius lines and prism cross-striations in human dental enamel after different acid etching regimes. *Arch. Oral Biol.* **49**, 45–52 (2004).
65. Desoutter, A. *et al.* Cross striation in human permanent and deciduous enamel measured with confocal Raman microscopy. *J. Raman Spectrosc.* **50**, 548–556 (2019).
66. Moorrees, C. F. A., Fanning, E. A. & Hunt, E. E. Jr. Age variation of formation stages for ten permanent teeth. *J. Dent. Res.* **42**, 1490–1502 (1963).
67. Demirjian, A., Goldstein, H. & Tanner, J. M. A new system of dental age assessment. *Hum. Biol.* **45**, 211–227 (1973).
68. Markowitz, M., Rotkin, L. & Rosen, J. Circadian rhythms of blood minerals in humans. *Science* **213**, 672 (1981).
69. Beynon, A. D., Dean, M. C. & Reid, D. J. On thick and thin enamel in hominoids. *Am. J. Phys. Anthropol.* **86**, 295–309 (1991).
70. Dean, C. *et al.* Growth processes in teeth distinguish modern humans from *Homo erectus* and earlier hominins. *Nature* **414**, 628–631 (2001).
71. Lacruz, R. S., Dean, M. C., Ramirez Rozzi, F. V. & Bromage, T. G. Megadontia, striae periodicity and patterns of enamel secretion in Plio-Pleistocene fossil hominins. *J. Anat.* **213**, 148–158 (2008).
72. Shellis, R. P. Variations in growth of the enamel crown in human teeth and a possible relationship between growth and enamel structure. *Arch. Oral Biol.* **29**, 697–705 (1984).
73. Dean, M. C. A histological method that can be used to estimate the time taken to form the crown of a permanent tooth. In *Forensic Microscopy for Skeletal Tissues: Methods and Protocols Vol. 915* (ed. Bell, L. S.) 89–100 (Humana Press, Berlin, 2012).
74. Guatelli-Steinberg, D., Floyd, B. A., Dean, M. C. & Reid, D. J. Enamel extension rate patterns in modern human teeth: two approaches designed to establish an integrated comparative context for fossil primates. *J. Hum. Evol.* **63**, 475–486 (2012).
75. Dean, M. C. & Cole, T. J. Human life history evolution explains dissociation between the timing of tooth eruption and peak rates of root growth. *PLoS ONE* **8**, e54534 (2013).
76. Dean, M. C., Humphrey, L., Groom, A. & Hassett, B. Variation in the timing of enamel formation in modern human deciduous canines. *Arch. Oral Biol.* **114**, 104719 (2020).
77. Beynon, A. D. & Wood, B. A. Patterns and rates of enamel growth in the molar teeth of early hominids. *Nature* **326**, 493–496 (1987).
78. Ramirez Rozzi, F. V. Tooth development in East African *Paranthropus*. *J. Hum. Evol.* **24**, 429–454 (1993).
79. Ramirez Rozzi, F. V. Time of crown formation in Plio-Pleistocene Hominid teeth. In *Structure, Function and Evolution of Teeth* (ed. Moggi-Cecchi, J.) 217–238 (International Institute for the Study of Man, Firenze, Italy, 1995).
80. Fooden, J. & Izor, R. J. Growth curves, dental emergence norms, and supplementary morphological observations in known-age captive orangutans. *Am. J. Primatol.* **5**, 285–301 (1983).
81. Zihlman, A., Bolter, D. & Boesch, C. Wild chimpanzee dentition and its implications for assessing life history in immature hominin fossils. *Proc. Natl. Acad. Sci. U. S. A.* **101**, 10541–10543 (2004).
82. Zihlman, A. L., Bolter, D. R. & Boesch, C. Skeletal and dental growth and development in chimpanzees of the Taï National Park, Côte D'Ivoire. *J. Zool.* **273**, 63–73 (2007).
83. Lockwood, C. A., Menter, C. G., Moggi-Cecchi, J. & Keyser, A. W. Extended male growth in a fossil hominin species. *Science* **318**, 1443 (2007).
84. Plavcan, J. M. Sexual dimorphism in hominin ancestors. In *The International Encyclopedia of Anthropology* (eds Callander, H. & Coleman, S.) 1–6 (American Cancer Society, New York, 2018).
85. Wood, B. A. *Koobi Fora research project Vol. 4* (Clarendon Press, Oxford, 1991).
86. Moggi-Cecchi, J., Menter, C., Boccone, S. & Keyser, A. Early hominin dental remains from the Plio-Pleistocene site of Drimolen, South Africa. *J. Hum. Evol.* **58**, 374–405 (2010).
87. Plavcan, J. M. A re-analysis of sex differences in landscape use in early hominins: a comment on Copeland and colleagues. *J. Hum. Evol.* **63**, 764–769 (2012).
88. Braga, J. & Thackeray, J. F. Early *Homo* at Kromdraai B: probabilistic and morphological analysis of the lower dentition. *C. R. Palevol* **2**, 269–279 (2003).
89. Lacruz, R. S. Enamel microstructure of the hominid KB 5223 from Kromdraai, South Africa. *Am. J. Phys. Anthropol.* **132**, 175–182 (2007).
90. Lacruz, R. S. & Bromage, T. G. Appositional enamel growth in molars of South African fossil hominids. *J. Anat.* **209**, 13–20 (2006).
91. Lacruz, R. S., Ramirez Rozzi, F. V. & Bromage, T. G. Variation in enamel development of South African fossil hominids. *J. Hum. Evol.* **51**, 580–590 (2006).
92. Wood, B. & Harrison, T. The evolutionary context of the first hominins. *Nature* **470**, 347–352 (2011).
93. Pampush, J. D. *et al.* Homoplasy and thick enamel in primates. *J. Hum. Evol.* **64**, 216–224 (2013).
94. Schwartz, G. T., McGrosky, A. & Strait, D. S. Fracture mechanics, enamel thickness and the evolution of molar form in hominins. *Biol. Lett.* **16**, 20190671 (2020).
95. Ziscovici, C., Lucas, P. W., Constantino, P. J., Bromage, T. G. & van Casteren, A. Sea otter dental enamel is highly resistant to chipping due to its microstructure. *Biol. Lett.* **10**, 20140484 (2014).
96. Beynon, A. D. & Wood, B. A. Variations in enamel thickness and structure in East African hominids. *Am. J. Phys. Anthropol.* **70**, 177–193 (1986).
97. Grine, F. E. & Franzen, J. L. Fossil hominid teeth from the Sangiran Dome (Java, Indonesia). *Cour. Forsch. Senckenberg* **171**, 75–103 (1994).
98. Dean, M. C. & Liversidge, H. M. Age estimation in fossil hominins: comparing dental development in early *Homo* with modern humans. *Ann. Hum. Biol.* **42**, 415–429 (2015).
99. Dean, M. C. Measures of maturation in early fossil hominins: events at the first transition from australopiths to early *Homo*. *Philos. Trans. R. Soc. B Biol. Sci.* **371**, 20150234 (2016).
100. Smith, B. H. The physiological age of KNM-WT 15000. In *The Nariokotome Homo erectus skeleton* (eds Leakey, R. E. & Walker, A.) 195–220 (Harvard University Press, Cambridge, 1993).
101. Vekua, A. *et al.* A New Skull of Early *Homo* from Dmanisi, Georgia. *Science* **297**, 85 (2002).
102. Copeland, S. R. *et al.* Strontium isotope evidence for landscape use by early hominins. *Nature* **474**, 76–78 (2011).
103. Sillen, A. & Balter, V. Strontium isotopic aspects of *Paranthropus robustus* teeth; implications for habitat, residence, and growth. *J. Hum. Evol.* **114**, 118–130 (2018).
104. Coleman, M. N. & Colbert, M. W. Technical note: CT thresholding protocols for taking measurements on three-dimensional models. *Am. J. Phys. Anthropol.* **133**, 723–725 (2007).
105. *Morphosource Database* <https://www.morphosource.org> (2020).

106. Dean, M. C., Le Cabec, A., Spiers, K., Zhang, Y. & Garrovoet, J. Incremental distribution of strontium and zinc in great ape and fossil hominin cementum using synchrotron X-ray fluorescence mapping. *J. R. Soc. Interface* **15**, 20170626 (2018).
107. Dean, M. C., Spiers, K. M., Garrovoet, J. & Le Cabec, A. Synchrotron X-ray fluorescence mapping of Ca, Sr and Zn at the neonatal line in human deciduous teeth reflects changing perinatal physiology. *Arch. Oral Biol.* **104**, 90–102 (2019).
108. Schroer, C. G. *et al.* Hard X-ray nanoprobes at beamline P06 at PETRA III. *Nucl. Instrum. Methods Phys. Res. Sect. B Beam Interact. Mater. At.* **616**, 93–97 (2010).
109. Boesenberg, U. *et al.* Fast X-ray microfluorescence imaging with submicrometer-resolution integrating a Maia detector at beamline P06 at PETRA III. *J. Synchrotron Radiat.* **23**, 1550–1560 (2016).
110. Kirkham, R. *et al.* The Maia spectroscopy detector system: engineering for integrated pulse capture, low-latency scanning and real-time processing. *AIP Conf. Proc.* **1234**, 240–243 (2010).
111. Falkenberg, G. *et al.* Large-scale high-resolution micro-XRF analysis of histological structures in the skin of the pigeon beak. *X Ray Spectrom.* **46**, 467–473 (2017).
112. Ryan, C. G. *et al.* Nuclear microprobe – synchrotron synergy: Towards integrated quantitative real-time elemental imaging using PIXE and SXRF. *Nucl. Microprobe Technol. Appl.* **231**, 183–188 (2005).
113. Weidmann, S. M., Weatherell, J. A. & Hamm, S. M. Variations of enamel density in sections of human teeth. *Arch. Oral Biol.* **12**, 85–97 (1967).
114. Boyde, A. Estimation of age at death of young human skeletal remains from incremental lines in the dental enamel. *Excerpta Med. Int. Congr. Ser.* **80**, 36–46 (1963).
115. Antoine, D., Hillson, S. & Dean, M. C. The developmental clock of dental enamel: a test for the periodicity of prism cross-striations in modern humans and an evaluation of the most likely sources of error in histological studies of this kind. *J. Anat.* **214**, 45–55 (2009).

## Acknowledgements

The SXRF work presented in this study was supported by DESY Project proposal I-20180047 and by the project CALIPSOplus under the Grant Agreement 730872 from the EU Framework Programme for Research and Innovation HORIZON 2020. We thank the DESY User Office, Dr. Gerald Falkenberg, Dr. Kathryn Spiers and those who have developed techniques employed in this study. We acknowledge the support to C.D. from the Calleva Foundation and to A.L.C. from The Max Planck Society. C.Z. and R.M. received support from the AESOP and AESOP+ consortia coordinated by José Braga. We sincerely acknowledge Stephany Potze for her help in 2015 at the Ditsong Nat. Museum Nat. History (DNMNH), Pretoria. We thank William Kimbel, Helen Liversidge, Ann Margvelashvili, Philip Rightmire, Friedemann Schrenk, Fred Spoor and Francis Thackeray for their help and support. For access to comparative  $\mu$ CT data of extant hominids, we thank Marie-Dominique Wandhammer (Mus. Zool. Strasbourg), Salvador Moyà-Solà, David M. Alba, Josep Fortuny and Alessandro Ursioli (Inst. Català Paleontol. Miquel Crusafont), Deborah Arbullo (Mus. Storia Nat. Trieste) and the Morphosource Database (<https://www.morphosource.org>). We extend our sincere thanks to the referees for their comments and suggestions.

## Author contributions

C.D., C.Z. and R.M. conceived and planned the study. C.Z., A.M. and R.M. performed the  $\mu$ XCT acquisitions and image processing. C.Z. performed  $\mu$ XCT-based measurements. C.D. prepared the specimen and collected the histological record data. J.G., A.L.C. and C.D. designed and performed the SXRF scans, J.G. and A.L.C. reconstructed the SXRF data and C.D. and A.L.C. analysed and interpreted the related data. M.T. provided curatorial assistance and granted access to fossil specimens curated at the DNMNH. C.D., C.Z. and R.M. wrote the paper with contributions from all authors.

## Competing interests

The authors declare no competing interests.

## Additional information

**Supplementary information** is available for this paper at <https://doi.org/10.1038/s41598-020-76032-2>.

**Correspondence** and requests for materials should be addressed to C.D.

**Reprints and permissions information** is available at [www.nature.com/reprints](http://www.nature.com/reprints).

**Publisher's note** Springer Nature remains neutral with regard to jurisdictional claims in published maps and institutional affiliations.



**Open Access** This article is licensed under a Creative Commons Attribution 4.0 International License, which permits use, sharing, adaptation, distribution and reproduction in any medium or format, as long as you give appropriate credit to the original author(s) and the source, provide a link to the Creative Commons licence, and indicate if changes were made. The images or other third party material in this article are included in the article's Creative Commons licence, unless indicated otherwise in a credit line to the material. If material is not included in the article's Creative Commons licence and your intended use is not permitted by statutory regulation or exceeds the permitted use, you will need to obtain permission directly from the copyright holder. To view a copy of this licence, visit <http://creativecommons.org/licenses/by/4.0/>.

© The Author(s) 2020

## SUPPLEMENTARY INFORMATION

### **Growth and development of the third permanent molar in *Paranthropus robustus* from Swartkrans, South Africa**

Christopher Dean<sup>1,2\*</sup>, Clément Zanolli<sup>3,4</sup>, Adeline Le Cabec<sup>3,5</sup>, Mirriam Tawane<sup>6</sup>, Jan Garrevoet<sup>7</sup>, Arnaud Mazurier<sup>8</sup> & Roberto Macchiarelli<sup>9,10</sup>

<sup>1</sup>Department of Earth Sciences, Natural History Museum, London, UK. <sup>2</sup>Department of Cell and Developmental Biology, University College London, London, UK. <sup>3</sup>Univ. Bordeaux, CNRS, MCC, PACEA, UMR 5199, F-33600 Pessac, France. <sup>4</sup>Department of Maxillofacial and Oral Surgery, Sefako Makgatho Health Sciences University, Ga-Rankuwa, Pretoria, South Africa; <sup>5</sup>Department of Human Evolution, Max Planck Institute for Evolutionary Anthropology, Leipzig, Germany. <sup>6</sup>Ditsong National Museum of Natural History, Pretoria, South Africa. <sup>7</sup>Deutsches Elektronen-Synchrotron DESY, Hamburg, Germany. <sup>8</sup>IC2MP, UMR 7285 CNRS, Université de Poitiers, Poitiers, France. <sup>9</sup>UMR 7194 CNRS, Muséum national d'Histoire naturelle, Musée de l'Homme, Paris, France. <sup>10</sup>Unité de Formation Géosciences, Université de Poitiers, Poitiers, France. \*email: [ucgacrd@ucl.ac.uk](mailto:ucgacrd@ucl.ac.uk)

#### **Supplementary Information includes:**

- Supplementary Texts S1-S5
- Supplementary Tables S1-S4
- Supplementary Figures S1-S17
- Supplementary References

## **Supplementary Text S1: M3 initiation times**

**Radiographic stages.** M3 development is the most variable of all tooth types. The time of initiation of M3 mineralisation can be determined either radiographically or from histology. Radiographically, a large empty crypt appears first, followed by the mineralising cusp tips. True initiation lies somewhere between these two radiographic stages but can never be determined precisely from radiographs. Radiographically, mean age of crypt appearance in modern humans ranges from 7.33 to 9.26 years<sup>1,2</sup> and mean age of M3 initiation between 7.92 to 9.69 years, but the range of ages is huge and may be from 5 to 12 years.

For the purposes of this study, 14 great apes, 11 of which were wild-shot museum specimens, with either a large empty lower M3 crypt or a crypt containing one or more mineralising cusp tips, were scored for radiographic formation stages of the premolars and first and second permanent molars in the same jaw quadrant (all radiographs are published in<sup>3-5</sup>). Where an empty M3 crypt was visible, or mineralising M3 cusps were already present, premolars and second permanent molars were between radiographic stages Crown complete and Root  $\frac{1}{4}$  formed. The M1 was consistently between radiographic stages Root  $\frac{3}{4}$  formed and Apex  $\frac{1}{2}$  closed (Supplementary Table S1, Supplementary Figs S1-S3).

In great apes of known age, the observed range of M3 initiation is tighter than in modern humans, likely in part because this occurs earlier in the growth period. For 5 captive chimpanzees of known age, the range was 2.99 to 4.61 years (mean: 3.5 years, SD: 0.64)<sup>6</sup>, and for a further 12 chimpanzees the mean was 3.64 years (SD: 0.33)<sup>7</sup>.

M3 cusp initiation was well underway in a free-living mountain gorilla at 5.31 years<sup>8</sup>. Reid and Guatelli-Steinberg<sup>9</sup> have noted that histological examination usually reveals earlier evidence of tooth initiation and estimated more advanced M3 initiation in 3 modern humans (range: 5.46-6.6 years). In comparing their data with early fossil hominins, they noted that it seemed likely early hominins more closely resembled modern humans in their range of initiation times than living great apes, "perhaps suggesting a grade shift in initiation times, at least for posterior teeth, early in human evolution"<sup>9</sup>.

Not much direct information is available from the early hominin fossil record. Only a small incipient M3 crypt is visible in a ~4-year-old early hominin (SK 63) from Swartkrans<sup>10</sup> and a large empty crypt is present in a 4.62-4.70-year-old early hominin (StW 151) from Sterkfontein<sup>11-13</sup>. The same is true in a slightly chronologically older early *Homo* mandible (KNM-ER 820) from Koobi Fora, Kenya<sup>14</sup>. No ages for M3 initiation in early hominins have ever been published. Many early hominins, however, do exist with M3s at later stages of development. On the basis of the evidence reviewed here, it seems clear there is insufficient evidence to determine a mean M3 initiation age for early hominins, or to improve on the broad estimate of Beynon and Dean<sup>15</sup> of ~5 years of age. However, a near-identical pattern, or sequence of premolar, M1 and M2 formation stages is observed in great apes and the few early hominins close to the stage of M3 initiation. Importantly, alongside this, new information is now available about the timing of events in premolar, M1 and M2 development, both earlier and later than M3 initiation in great apes and early hominins<sup>8,12,13</sup> and suggests M3 initiation occurred sometime between 4 and 7 years of age in early hominins.

## **Supplementary Text S2: Specimen description**

The crown of SK 835, a maxillary left M3, consists of three separate fragments that can be fitted together with reasonable accuracy (Supplementary Fig. S5). Two mesial fragments comprise the paracone and protocone, and a third fragment comprises the distal metacone and hypocone. Each of the three roots are also separate from each other and the crown, but can be joined together at the base of the crown, although there is considerable damage around the cervix and root trunk. The palatal root consists of a coronal segment that extends



up within the enamel cap, with a small portion of the last-formed cervical enamel attached to it. This is the only true continuity between the crown and root. The palatal root is, however, incomplete and fractured obliquely across its apical third. The mesiobuccal root is incomplete at the buccal cervix and cannot be joined to the crown, but it does preserve the root apex on both its mesial and lingual surfaces. The distobuccal root is made up of three small cervical fragments, two palatal and one buccal, previously glued together. The buccal fragment includes a small portion of cervical enamel marking the crown-root junction. This root is almost complete to the apex buccally, but is damaged lingually (Supplementary Figs S5-S7).

The two mesial crown fragments (paracone and protocone), along with the palatal root, were located together in the best fit possible using cyanoacrylate cement. The dentine horns within both mesial cusps were identified on  $\mu$ XCT scans and the points above them marked on the enamel surface overlying these (Supplementary Fig. S4). A plane of section was identified that passed through both paracone and protocone dentine horns and through the long axis of the palatal root (Supplementary Fig. S5). A decision was made to section the mesiobuccal and distobuccal roots separately. Buccolingual longitudinal planes of section through the mesiobuccal and distobuccal roots were defined with the intention of maximising the root width, root canal and root length captured within each section (Supplementary Figs S6, S7). The enamel and dentine surfaces along the planes of section were coated with cyanoacrylate cement and allowed to dry for 48 hours to prevent any brittle tissue flaking off during the cutting and polishing process. This is also easily dissolved off post-sectioning enabling easy reconstruction of the cleaned blocks whereas embedding the whole tooth in, for example, methyl methacrylate, risks greater damage when de-embedding is required.

### Supplementary Text S3: Enamel histology

**Cuspal enamel formation time and rate.** Digital photo-montages were constructed of the SK 835 enamel cap. Four prism paths were identified in cuspal enamel where good daily prism cross striations could be tracked from the EDJ to the enamel surface. These are indicated in sequence from left (palatal) to right (buccal) in Supplementary Figure S7 by the four red arrows 'a'-'d'. These were: (a) palatal to the protocone dentine horn, 1200  $\mu$ m along the EDJ avoiding poorly preserved enamel; (b) directly over the protocone dentine horn, alongside a crack in this position; (c) directly over the paracone dentine horn; and (d) immediately buccal to the axial paracone dentine horn.

Decussation in the enamel was minimal in outer enamel but still apparent, especially in inner enamel. Each straight-line prism path was divided into 100- $\mu$ m segments or zones and direct counts of daily enamel cross striations that weave from side to side within and between zones were made and cumulated. The total cumulative counts along each prism path between zero days at the EDJ and the last-formed occlusal enamel at the surface were respectively 580, 533, 555 and 575 days, with the greatest counts on the palatal aspect of the protocone (580 days) and buccal of the paracone (575 days). However, only the first prism track (580 days) emerges at an unworn enamel surface. For all four prism path trajectories combined, a second order polynomial regression plot describes the cumulative days of enamel formation (Supplementary Fig. S8). Note that in Supplementary Figure S8 the distance from the EDJ is plotted on the Y axis, but in the equations that follow, Y corresponds to the formation time in days.

For all four trajectories combined, the time (Y) taken to form a given thickness of occlusal enamel (X) equals:

$$Y = 12.651 + .284X - 3.459e^{-5}X^2 \quad (R^2 = .979). \quad (\text{Eq. 1})$$

Lower 95% confidence interval:

$$Y = -.197 + .265X - 4.063e^{-5}X^2.$$

Upper 95% confidence interval:

$$Y = 25.498 + .303X - 2.856e^{-5}X^2.$$

When the slower palatal protocone trajectory is excluded, the following second order polynomial regression plot describes the average cumulative days of enamel formation across the remaining three trajectories:

$$Y = 18.029 + .276X - 2.866e^{-5}X^2 (R^2 = .987)$$

To provide a better sequential profile of variation in daily enamel formation rates through the cuspal enamel, 60-day zones were then defined between the EDJ and the enamel surface along each of the four prism paths. Within each 60-day zone, groups of 6 cross striations were marked that define 5 days enamel growth. The average linear daily rate of enamel formation was calculated by dividing the distance along a prism from the first to the sixth cross striations by 5. This was repeated as many times as possible within each 60-day zone, where a minimum 8 times and a maximum 23 times were possible. While it would have been desirable to divide the cuspal enamel into smaller 30-day (monthly) zones, in some places too few measurements were possible to generate meaningful box plots.

The profile of changing enamel rates through these 60-day zones is shown in Supplementary Fig. S9; that of rate changes in a modern human M1, M2 and M3 from the same individual, but divided into 30-day zones, appears for comparison in Supplementary Fig. S10 and illustrates the typical M1-M3 declining gradient in modern humans but with similar rates at the EDJ. In SK 835, the protocone and paracone cusp tips are both slightly worn, so, apart from the most palatally positioned prism path in the protocone, no true outer enamel remains. Average rates close to the EDJ were 3.28  $\mu\text{m}/\text{d}$  and, in the protocone, rose to 8.28  $\mu\text{m}/\text{d}$  (SD: 0.406, range: 7.5-9.0  $\mu\text{m}/\text{d}$ ) in outer enamel before reducing again to  $\sim 7.3 \pm 0.5$   $\mu\text{m}/\text{d}$  in the last 120 days of enamel formation at the surface, which became aprismatic here.

When summarised as inner, middle and outer regions of equally thick cuspal enamel, the overall mean values for all cross striation spacings within the palatal aspect of the protocone are 3.99, 5.68 and 7.95  $\mu\text{m}$ , respectively. On the occlusal aspect of the protocone, they are slightly less (3.55, 4.94, 6.62  $\mu\text{m}$ ). Equivalent values in the paracone for inner, middle and outer thirds of occlusal enamel of equal thickness are slightly less than those for the protocone. The overall mean value of all cross striation spacings measured in the protocone is 5.56  $\mu\text{m}$  (SD: 1.63  $\mu\text{m}$ ) and of all cross striation spacings in the paracone is 4.89  $\mu\text{m}$  (SD: 1.24  $\mu\text{m}$ ). The overall mean value of cross striation spacings measured in the fastest trajectory of the protocone (palatal aspect) is 6.02  $\mu\text{m}$  (SD: 1.75  $\mu\text{m}$ ) and in the fastest trajectory of the paracone (occlusal aspect) is 4.97  $\mu\text{m}$  (SD: 1.51  $\mu\text{m}$ ).

**Enamel formation rates at the EDJ.** Measurements of daily enamel cross striation spacings in SK 835 were made in the same way at different positions along the EDJ between the dentine horn and the enamel cervix. At four positions spaced equally between the dentine horn and enamel cervix, measurements were made within the first 200  $\mu\text{m}$  from the EDJ. The grand mean of 54 repeated 5-day averages within enamel 200  $\mu\text{m}$  from the EDJ was 3.28  $\mu\text{m}/\text{day}$  (SD: 0.310, range: 2.6-3.9  $\mu\text{m}/\text{day}$ ). This was rounded to 3.3  $\mu\text{m}/\text{day}$ , which equals 61 days to form a 200- $\mu\text{m}$  thickness of enamel close to the EDJ.

**Total enamel formation time.** It was not possible to image regular long-period striae of Retzius through the whole of the lateral enamel in either the protocone or the paracone. Moreover, counts of daily cross striations between regular long-period striae associated with perikymata at the enamel surface were inconsistent between the protocone and paracone. Direct counts between adjacent long-period striae in the protocone numbered 6 or 7 days (Supplementary Fig. S11). The average of five long-period stria widths was 31.9  $\mu\text{m}$  and the average of ten 5-day groups of cross striations within these striae was 4.91  $\mu\text{m}$ ,

giving an average periodicity of 6.496 (6.5) days. It was not then possible to say if the periodicity is 6 or 7 days, since periodicities are by definition always expressed in whole days. Regions of the paracone cervix complicate this picture further. Here again, there are clear daily cross striations as well as alternating varicosities and constrictions with apparently well-expressed regular long-period increments, some of which can be associated with what might be construed as surface perikymata (Supplementary Fig. S11). However, the periodicity is twice, if not more than twice, that observed in the protocone cervix. Accordingly, in this study stria counts and long-period stria periodicity were not used in any calculations of crown formation time.

The methods used here for calculating total enamel formation time have been described in previous studies<sup>16-19</sup> and are derived from those originally described by Boyde<sup>20,21</sup>, Risnes<sup>22</sup> and Antoine and co-workers<sup>23</sup>. These were used here to calculate cusp-specific enamel formation times for both the protocone and the incompletely preserved paracone. A 200- $\mu\text{m}$  long prism path representing 61 days enamel formation was first measured from the tip of the dentine horn. From this point, a line was extended back to intersect with the EDJ either along or parallel with an accentuated incremental marking. The length of enamel along the EDJ from the dentine horn to this point of intersection formed in 61 days. This length along the EDJ, divided by 61 days, defines the extension rate between the dentine horn and the point of intersection at the EDJ. Again, from this point of intersection at the EDJ a second 200- $\mu\text{m}$  prism path was extended out into enamel, and the same procedure repeated. Successive 61-day units of time defined in this way between the dentine horn and the enamel cervix were then cumulated to give a total cuspal enamel formation time. In the protocone there were  $15 \times 61$  day 200- $\mu\text{m}$  increments from cusp to cervix, plus a 30-day half increment which equals  $15 \times 61 + 30 = 945$  days, or 2.59 years, of enamel formation. In the paracone, there were  $9 \times 61$  day 200- $\mu\text{m}$  increments = 549 days, or 1.50 years, of enamel formation to the incomplete enamel cervix.

**Enamel extension rates.** The extension rate is a measure of the rate at which new ameloblasts differentiated along the EDJ<sup>24</sup>. In the protocone, initial cuspal extension rates were 30  $\mu\text{m}/\text{day}$ , dropping to 14  $\mu\text{m}/\text{day}$  in the first 61 days of crown formation, and then to 7  $\mu\text{m}/\text{day}$  by  $\sim 240$  days. Thereafter, extension rates in this cusp remained constant at  $\sim 7$   $\mu\text{m}/\text{day}$  for the remainder of crown formation. In the paracone, extension rates were initially less at 21  $\mu\text{m}/\text{day}$ , dropping immediately to 9  $\mu\text{m}/\text{day}$  within 61 days, and then 6-7  $\mu\text{m}/\text{day}$  as in the protocone. This slower extension rate in the paracone cusp tip than in the protocone may be an indication of slight section obliquity here clipping off the peak of the paracone dentine horn. This has implications for estimating paracone initiation time relative to the protocone.

**Initiation of the paracone and protocone.** The SXRF overview scans reveal a series of clear Sr bands both in the enamel and dentine of this specimen (Fig. 5). Alternating regions of Sr enrichment and depletion can be identified with more intense Sr bands superimposed upon this underlying pattern. Within the enamel and the root dentine, Sr bands allow cusps and roots forming at the same time to be cross-matched. In the crown, many of the Sr bands were associated with accentuated markings visible with transmitted light microscopy (TLM). Because the accentuated lines in enamel were more clearly defined and less diffuse than the Sr bands, they were used to align protocone and paracone formation. A number of accentuated lines, each of about equal intensity, run through the enamel. Most of these lines can be tracked back to the EDJ and matched to a time corresponding to the closest 61 day increment as defined above (Supplementary Fig. S7, white arrows). Almost all the accentuated lines appear bright in polarised light except a few strong lines that are dark. Lines that form within the cuspal enamel run between cusps,

but those that form after ~600 days are contained only within the lateral enamel and emerge at the protocone or paracone surface (Supplementary Fig. S7). In general, the mid-cuspal enamel and lateral enamel contain the most accentuated markings. Enamel formed between ~400 days and ~500 days and between ~670 days and ~850 days appeared worst affected by these, what are assumed to be, stress-related markings.

Four accentuated markings within enamel were identified in SK 835 that could be clearly seen running through the protocone, occlusal enamel and paracone (Supplementary Fig. S7, white arrows). These were used as common temporal registration markings. Daily cross striation counts from the EDJ to the first marking, and then between subsequent accentuated markings, were used to cross match enamel growth in the protocone with that in the paracone. Direct counts of daily incremental markings in the protocone to the first-formed bright accentuated line lying closest to the EDJ (Supplementary Fig. S7) were 210 days. Direct counts to the same corresponding line in the paracone were 190 days. This suggests the protocone began to mineralise ~20 days before the paracone. A second matching pair of accentuated lines occurs at 287 days in the protocone and 260 days in the paracone, suggesting a greater 27-day difference. It is unusual, but not unknown, for the protocone to initiate before the paracone and, on the face of it, that is what appears to have been the case in SK 835. But the difference observed of 20-30 days between the two cusps in this section is relatively small, and the error of making direct counts in decussating cuspal enamel, and with the possibility of some section obliquity at the paracone dentine horn, inclines to the safer assumption that both cusps initiated very close together in time. It follows that in the plots of EDJ length against tooth formation time both cusps were assumed to initiate at the same time (Figs 4, 7).

#### **Supplementary Text S4: Dentine histology**

**Regions of interest.** Digital photo-montages were first constructed of each root at low power between the most cervical and apically preserved root dentine of SK 835. Eight regions of interest were chosen that expressed good daily dentine increments between the root surface and to a depth of at least 200  $\mu\text{m}$  into dentine (Supplementary Fig. S7, yellow boxes). These were in the mid-root and cervical third of the palatal root, the buccal and lingual mid-root, and the buccal apical region of the mesiobuccal root, and the mid-root and apical third of the distobuccal root. Higher power digital photomontages were constructed of these regions of interest.

**Daily rates of root dentine formation.** Daily dentine rates were measured in the same way as those in enamel. Six successive daily dentine increments were marked and the distance across them divided by 5. The mean of 340 such 5-day averages measured in 7 of the 8 regions of interest all within a 200- $\mu\text{m}$  zone from the cement dentine junction (CDJ) was 2.49  $\mu\text{m}$  (SD: 0.499, range: 1.62-4.0  $\mu\text{m}$ ). The average time to form a 200- $\mu\text{m}$  thickness of root dentine from the CDJ was, therefore, estimated to be  $200 / 2.49 = 80.32$  days, which was rounded to 80 days (Supplementary Fig. S12). Additional measurements of daily dentine rates were possible between the CDJ and the lateral margin of the apical canal of the mesiobuccal root (Supplementary Fig. S7). Here, across 1040  $\mu\text{m}$  of apical dentine, rates rose gradually away from the CDJ, and then reduced again towards the apical canal. The average rate was 2.87  $\mu\text{m}/\text{day}$  (SD: 0.469, range: 1.78-3.65  $\mu\text{m}/\text{day}$ ). On this basis, apical closure from a stage of root formation equivalent to radiographic Root length complete (RC) could be estimated in this root.

**Accentuated lines in the root dentine.** A prominent Sr line visible in the SXRF scans was chosen as a marker of root formation common to all roots (Fig. 5 and Supplementary Fig. S7, orange arrows). A separate group of closely spaced accentuated lines visible in TLM can also be identified in the apical third of all three roots in TLM (Supplementary

Fig. S7, blue arrows). At higher power, these appear alternately either bright or dark in TLM, and are either more closely spaced or more widely separated from each other as if irregular periods of slowing are followed by catch-up periods of dentine formation (Supplementary Fig. S13). Together, they form a distinct pattern that can be accurately cross-matched between all three roots. In practice, the prominent Sr line visible in the SXRF images proved the most practical way to match root formation occurring at the same time.

Root formation in the palatal root from the protocone cervix (the last formed enamel) was calculated up to the Sr marker line. Root formation both before and beyond the Sr marker line, could also be calculated in the distobuccal root. The cervical enamel in the distobuccal root is poorly preserved and cannot be reliably linked to enamel in the rest of the crown. Moreover, the distobuccal root apex is incomplete, such that dentine in this root still falls short of the last formed apical root dentine (Fig. 5 and Supplementary Fig. S7). However, the distobuccal root contains the longest record of root growth and can be aligned with the other two forming roots using the Sr marker line. Only the mesiobuccal root has a clear well-formed closed apex, but this root does not preserve an enamel cervix and is a slightly shorter root. Root formation in the mesiobuccal root can, however, also be cross-matched with root formation in the other two roots using the Sr marker band. Distobuccal root formation from the accentuated Sr marker line (Fig. 5 and Supplementary Fig. S7, orange arrows) to the radiographic stage of Root length complete (RC) was estimated using 80-day time segments along the CDJ (see below). However, the final period of dentine formation (Apex closure) was estimated from direct counts of daily increments across the thickness of the apical primary dentine in the mesiobuccal root. In this way, an estimate of total root formation time from the protocone enamel cervix to the accentuated Sr marker line (Supplementary Fig. S7, orange arrows), and then onwards in the distobuccal root and finally through mesiobuccal root to apical closure, could be represented as a composite plot of increasing tooth height along the EDJ against tooth formation time (Fig. 4).

**Total root formation time.** In the palatal root, from the junction of the last formed enamel and first formed root dentine at the cervix, a line was drawn along the direction of dentine tubules 200  $\mu\text{m}$  deep into dentine. From this point, accentuated growth lines in dentine, marking the former position of the forming dentine front, were used to track a second line back to intersect the CDJ at the root surface. The length along the CDJ, between the start point at the cervix and this intersection at the CDJ, took 80 days to form. Starting again from this point of intersection at the CDJ, the process was repeated as far as possible towards the root apex. The sum of the consecutive 80-day time segments equals the total root formation time when both the enamel cervix and the apical root margin are preserved. This procedure is illustrated in Supplementary Fig. S14 and was repeated along the outer CDJ in each of the three roots of SK 835, but was only possible within the limitations of root preservation.

There were 9 consecutive 80-day segments in the palatal protocone root to the fractured root end ( $9 \times 80 = 720$  days, or 1.97 years). However, beyond protocone enamel completion at 945 days, there were only  $6 \times 80$ -day segments prior to the Sr marker line ( $7 \times 80 = 560$  days, or 1.53 years). The Sr line in the palatal and distobuccal roots can therefore be cross-matched at  $945 + 560 = 1505$  days, or 4.123 years (Supplementary Fig. S7, orange arrows). In the distobuccal root, there were a total of  $19 \times 80$ -day segments from a reconstructed but poorly defined enamel cervix to the fractured root apex ( $19 \times 80 = 1520$  days, or 4.16 years). However, there were only  $12 \times 80$ -day segments ( $12 \times 80 = 960$  days, or 2.63 years) beyond the Sr line in the distobuccal root, excluding apex closure. Total tooth formation time prior to apex closure in the distobuccal root then equals  $1505 + 960 = 2465$  days, or 6.75 years. If average rates of root dentine formation were

slightly lower or higher (75 or 85 days to form 200  $\mu\text{m}$  rather than 80 days) root completion would have been 6.75 years  $\pm$  95 days. It was not possible to estimate apex closure time in the distobuccal root. However, in the mesiobuccal root, dentine thickness between the CDJ and the lateral aspect of the completed apical canal measured 1040  $\mu\text{m}$ . At an average daily formation rate of 2.87  $\mu\text{m}/\text{day}$  measured within this region, this is equivalent to 362 days, or about a year. What this might have been in the likely slightly longer and usually last-completed palatal root remains unknown. It may also have taken less time than this for the distobuccal root apex to close completely. Nonetheless, it suggests that total tooth formation time would almost certainly have been greater than 7 years, and even as much as 7.75 years in SK 835.

Figure 4 shows the cumulative growth curve for increasing distance along the EDJ/CDJ ( $\mu\text{m}$ ) against formation time (years) expressed here as a 5<sup>th</sup> order polynomial that allows formation time (Y) to be predicted from a known value of EDJ/CDJ length (X) as follows:

$$Y = .018 + 8.875e^{-5}X + 4.414e^{-8}X^2 - 3.009e^{-12}X^3 + 4.581e^{-17}X^4 + 6.494e^{-22}X^5. \quad (\text{Eq. 2})$$

$$(R^2 = .993)$$

Supplementary Fig. S15 represents the incremental growth of SK 835 expressed differently, with successive ages given from the time of M3 initiation shown for  $\frac{1}{4}$  fractions of time for crown and root formation, and  $\frac{1}{4}$  fractions of height for crown and root formation.

**Root extension rates.** As in enamel, the root extension rate (in this case, the rate at which new odontoblasts differentiate along the CDJ) can be estimated by dividing a defined length of the CDJ by the time taken to form it. The length of the CDJ formed in each 80-day segment varies considerably in SK 835. Close to the cervix, root dentine extension rate calculations in all three roots were close to the rates calculated at the end of enamel formation ( $\sim 9 \mu\text{m}/\text{day}$ ). Thereafter there was a swift rise to a peak rate of 15  $\mu\text{m}/\text{day}$ , in the mesiobuccal root, and to 19  $\mu\text{m}/\text{day}$ , in both the palatal and distobuccal roots between 3.5 and 4 years after protocone initiation. Following this, rates slowed again towards the root apex. The last of the 80-day segments of the mesiobuccal root, just prior to apex formation, extended at 3-5  $\mu\text{m}/\text{day}$ . Thereafter, the strongly curving contour of the rounded root apex, combined with poor expression of accentuated forming-front markings, makes extension rate estimates beyond the stage of root length complete (RC) less reliable by this method. The time taken for apical closure of the mesiobuccal and distobuccal roots was therefore estimated on the basis of direct counts of daily dentine increments and an observed average daily rate in apical dentine of 2.87  $\mu\text{m}/\text{day}$ .

#### **Supplementary Text S5: Enamel thickness assessment.**

By using  $\mu\text{XCT}$  records, the 2D relative enamel thickness (RET) and absolute crown strength (ACS) indices were comparatively assessed in SK 835 and in other *P. robustus* and extant hominid M3s (Supplementary Table S3). 2D RET provides an estimation of crown enamel proportions<sup>25</sup>, while ACS gives an estimation of tooth strength, i.e., of resistance to fracture<sup>26</sup>. The biplot of 2D RET vs. ACS is shown in Supplementary Fig. S16. The extant apes have thin to moderately thin enamel (as attested by their 2D RET values), associated with low ACS values. Modern humans, located below the regression line, also have low ACS values, suggesting that their thick enamel (comparable to the 2D RET values of *P. robustus*) are less adapted to resist fractures than the thick enamelled condition of *P. robustus* (including SK 835), the latter taxon exhibiting markedly higher ACS values.

## Supplementary Tables

**Supplementary Table S1.** Radiographic scores for lower teeth represented in Supplementary Figs S1-S3.

Taxon	Number	Pm3	Pm4	M1	M2	M3
<i>Gorilla</i>	18911	Ri	R1/4	RC	Ri	Crypt small
<i>Gorilla</i>	1939-937	CC	Ri	A1/2	CC	Ci
<i>Gorilla</i>	29112	CC	CC	RC	CC	Ci
<i>Gorilla</i>	Os Hill RCS	C3/4	CC	R3/4	CC	Ci
<i>Gorilla</i>	1268/650	C3/4	C3/4	R3/4	C3/4	Crypt small
<i>Pongo</i>	1948-831	CC	CC	RC	CC	Ci
<i>Pongo</i>	1852-3212	CC	CC	RC	CC	Ci
<i>Pongo</i>	1976-1410	Ri	R1/4	A1/2	Ri	Ci
<i>Pongo</i>	A65-13	CC	CC	R3/4	CC	Crypt large
<i>Pan</i>	M675	R1/4	R1/4	A1/2	Ri	Ci
<i>Pan</i>	1939-1002	CC	CC	A1/2	CC	Ci
<i>Pan</i>	M855	CC	Ri	RC	CC	Crypt large
<i>Pan</i>	M507	R1/4	R1/4	A1/2	Ri	Ci
<i>Pan</i>	M847	Ri	Ri	A1/2	Ri	Ci

**Supplementary Table S2.** Predicted formation times for successive cumulative 1 mm lengths along the EDJ and CDJ in SK 835 M3.

EDJ/CDJ length ( $\mu\text{m}$ )	Predicted time (years)	Predicted time (days)
1000	0.044	16
2000	0.310	113
3000	0.602	220
4000	0.914	334
5000	1.239	452
6000	1.570	573
7000	1.900	693
8000	2.223	811
9000	2.532	924
10000	2.825	1031
11000	3.095	1130
12000	3.343	1220
13000	3.565	1301
14000	3.764	1374
15000	3.943	1439
16000	4.106	1499
17000	4.260	1555
18000	4.417	1612

EDJ/CDJ length ( $\mu\text{m}$ )	Predicted time (years)	Predicted time (days)
19000	4.588	1675
20000	4.790	1748
21000	5.042	1840
23000	5.790	2113
24000	6.343	2315
25000	7.060	2577
26000	7.979	2912

**Supplementary Table S3.** Relative enamel thickness (2D RET) and absolute crown strength (ACS) indices assessed in *P. robustus* and extant hominid M3s.

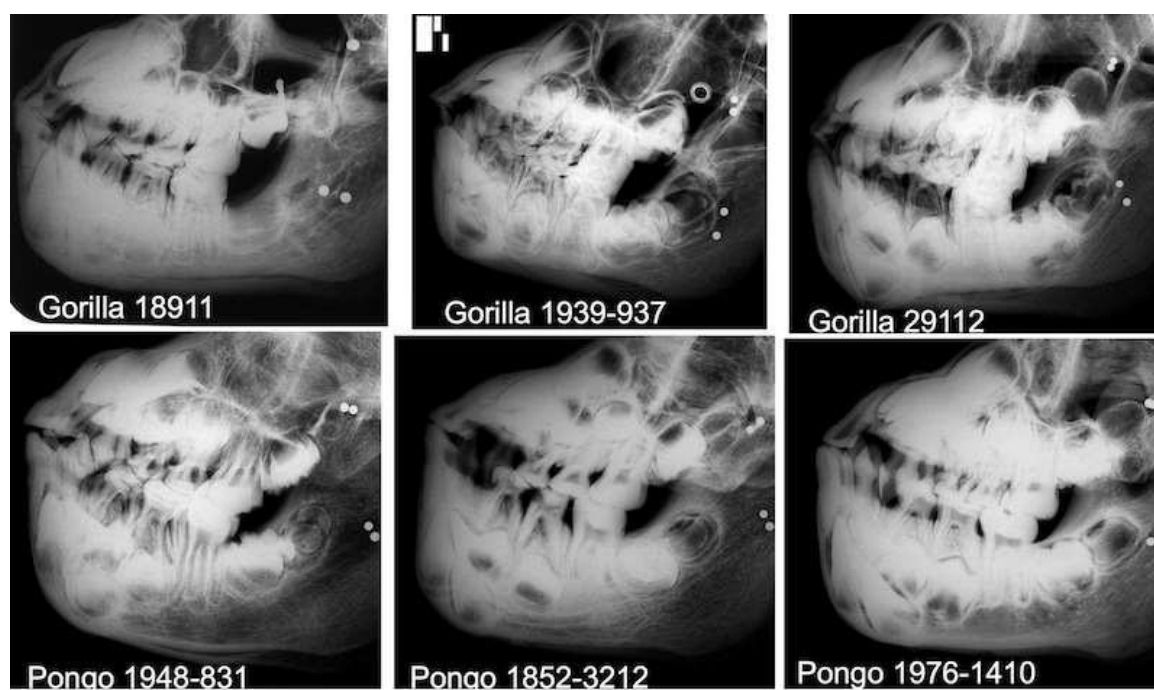
Taxon	Specimen	2D RET	ACS	References
<i>P. robustus</i>	SK 13-14	36.53	4.54	original data
<i>P. robustus</i>	SK 31	22.71	3.91	original data
<i>P. robustus</i>	SK 48	29.64	4.32	original data
<i>P. robustus</i>	SK 49	29.57	4.23	original data
<i>P. robustus</i>	SK 105	25.32	3.94	original data
<i>P. robustus</i>	SK 831a	22.36	3.81	original data
<i>P. robustus</i>	SK 835	28.95	3.99	original data
<i>P. robustus</i>	SK 836	24.27	4.17	original data
<i>P. robustus</i>	SKW 11	25.96	4.27	original data
<i>P. robustus</i>	TM 1517C	30.57	4.12	original data
<i>H. sapiens</i>	ind1	25.77	2.50	original data
<i>H. sapiens</i>	ind2	28.69	2.80	original data
<i>H. sapiens</i>	ind3	26.17	2.94	original data
<i>H. sapiens</i>	ind4	23.17	2.33	original data
<i>Pan</i>	IPS5698	11.36	1.62	original data
<i>Pan</i>	MCZ-9493	13.62	1.60	<sup>27</sup>
<i>Pan</i>	MCZ-23167	13.87	1.98	<sup>27</sup>
<i>Pan</i>	MCZ-38018	12.06	1.74	<sup>27</sup>
<i>Gorilla</i>	MCZ-14750	14.01	2.80	<sup>27</sup>
<i>Gorilla</i>	MCZ-37264	12.81	2.48	<sup>27</sup>
<i>Gorilla</i>	MCZ-37266	15.88	2.43	<sup>27</sup>
<i>Gorilla</i>	MCZ-38326	10.65	2.40	<sup>27</sup>
<i>Pongo</i>	Sbg_903	14.16	2.24	original data
<i>Pongo</i>	MZS-2632	13.78	2.47	original data
<i>Pongo</i>	MNSNT Pongo1	14.29	2.25	original data
<i>Pongo</i>	IPS9031	16.86	2.42	original data



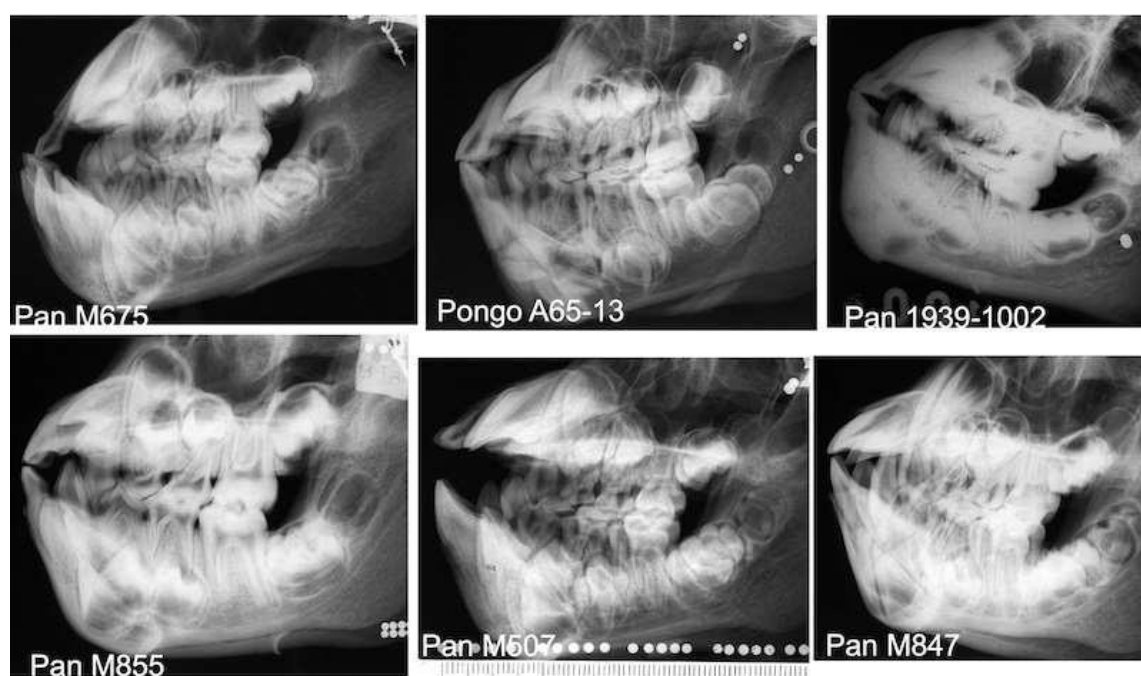
**Supplementary Table S4.** Plio-Pleistocene hominins in which M3 development is incomplete ordered here by M3 stage that best approximates the proportion of crown or root height/length formed. Stages were estimated from the literature and/or from casts/images. A minimum and a maximum relative dental age (RDA in years) based on M3 initiation at 4 years and at 7 years respectively, likely bracket the true age at death.

Specimen accession number	Taxon	Provenance	M3 stage	Min M3 RDA	Max M3 RDA
StW 151 <sup>11</sup>	<i>A. africanus</i>	South Africa	Crypt	4.0	7.0
KNM-ER 820 <sup>14,28,29</sup>	early <i>Homo</i>	Kenya	Crypt	4.0	7.0
Sts 8 <sup>30</sup>	<i>A. africanus</i>	South Africa	CC	2.59+4=6.59	2.59+7=9.59
MH1 <sup>31-33</sup>	<i>A. sediba</i>	South Africa	CC	2.59+4=6.59	2.59+7=9.59
SK 843 <sup>30</sup>	<i>P. robustus</i>	South Africa	CC	2.59+4=6.59	2.59+7=9.59
KNM-WT 17400 <sup>34</sup>	<i>P. boisei</i>	Kenya	CC	2.59+4=6.59	2.59+7=9.59
KNM-ER 62000 <sup>35</sup>	<i>H. rudolfensis</i>	Kenya	CC	2.59+4=6.59	2.59+7=9.59
KNM-WT 15000 <sup>36</sup>	<i>H. erectus</i> s.l.	Kenya	CC	2.59+4=6.59	2.59+7=9.59
A.L. 486-1 <sup>37</sup>	<i>A. afarensis</i>	Ethiopia	R1/2	4.26+4=8.26	4.26+7=11.26
TM 1511 <sup>30</sup>	<i>A. africanus</i>	South Africa	R1/2	4.26+4=8.26	4.26+7=11.26
SK 13/14 <sup>30</sup>	<i>P. robustus</i>	South Africa	R1/2	4.26+4=8.26	4.26+7=11.26
DNH 10 <sup>38</sup>	<i>P. robustus</i>	South Africa	R1/2	4.26+4=8.26	4.26+7=11.26
OH 13 <sup>30,39</sup>	<i>H. habilis</i>	Tanzania	R1/2	4.26+4=8.26	4.26+7=11.26
OH 16 <sup>39</sup>	<i>H. habilis</i>	Tanzania	R1/2	4.26+4=8.26	4.26+7=11.26
D2700 / D2735 <sup>40,41</sup>	<i>H. erectus</i> s.l.	Georgia	R1/2	4.26+4=8.26	4.26+7=11.26
Sts 52/53 <sup>30</sup>	<i>A. africanus</i>	South Africa	R3/4	5.04+4=9.04	5.04+7=12.04
TM 1517 <sup>42</sup>	<i>P. robustus</i>	South Africa	R3/4	5.04+4=9.04	5.04+7=12.04
OH 5 <sup>30,43</sup>	<i>P. boisei</i>	Tanzania	R3/4	5.04+4=9.04	5.04+7=12.04
KNM-CH1 <sup>44</sup>	<i>P. boisei</i>	Kenya	R3/4	5.04+4=9.04	5.04+7=12.04
KNM-ER 992 <sup>28,29</sup>	<i>H. erectus</i> s.l.	Kenya	A1/2	6.67+4=10.67	6.67+7=13.67
Sangiran 4 <sup>45,46</sup>	<i>H. erectus</i> s.l.	Indonesia	A1/2	6.67+4=10.67	6.67+7=13.67

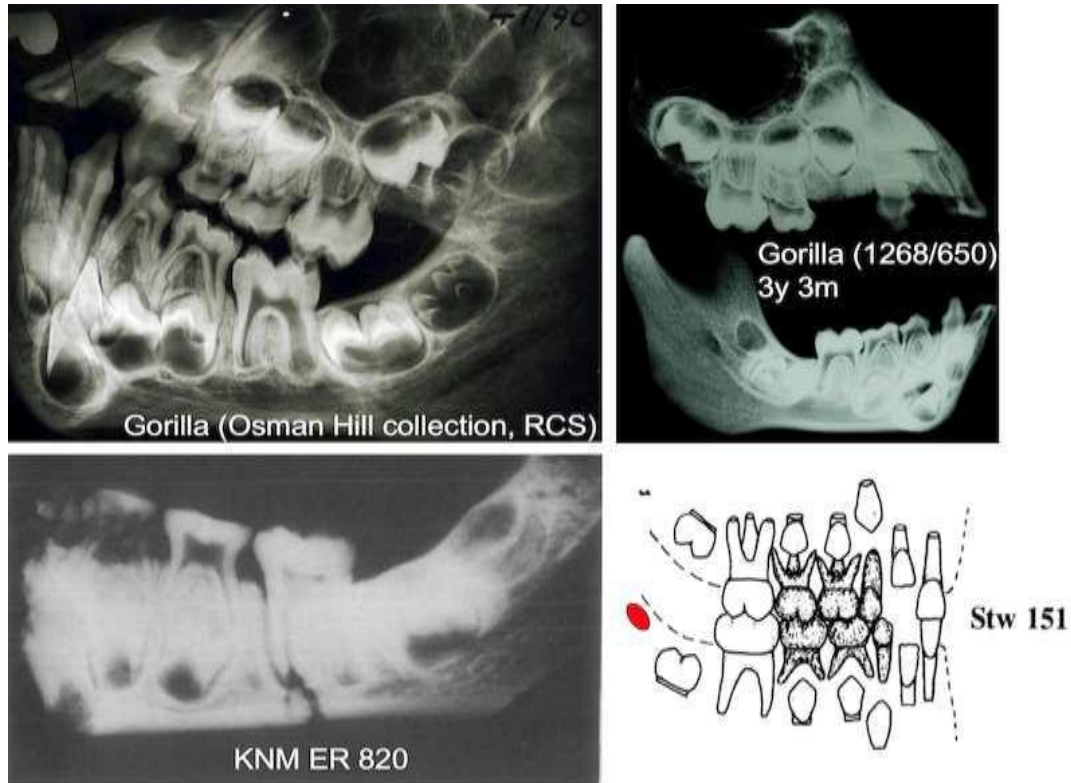
## Supplementary Figures



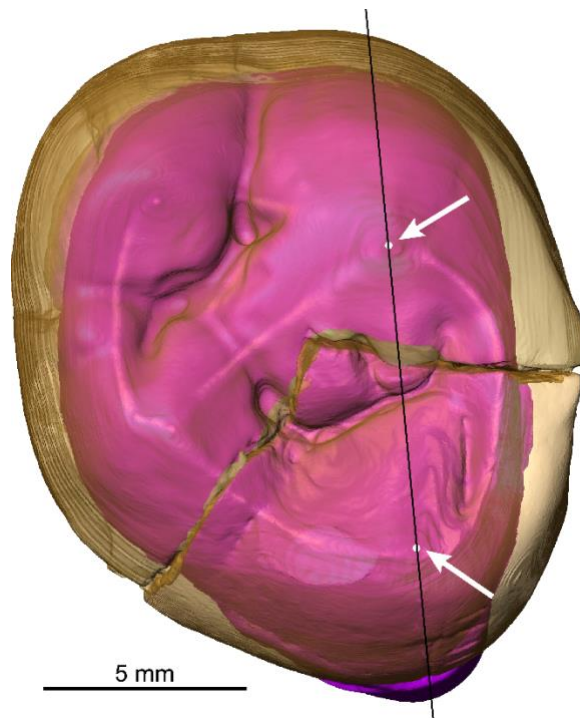
**Supplementary Figure S1.** *Gorilla* and *Pongo* at the stage of upper and/or lower M3 initiation<sup>4</sup>.



**Supplementary Figure S2.** *Pan* and *Pongo* at the stage of upper and/or lower M3 initiation<sup>4</sup>.



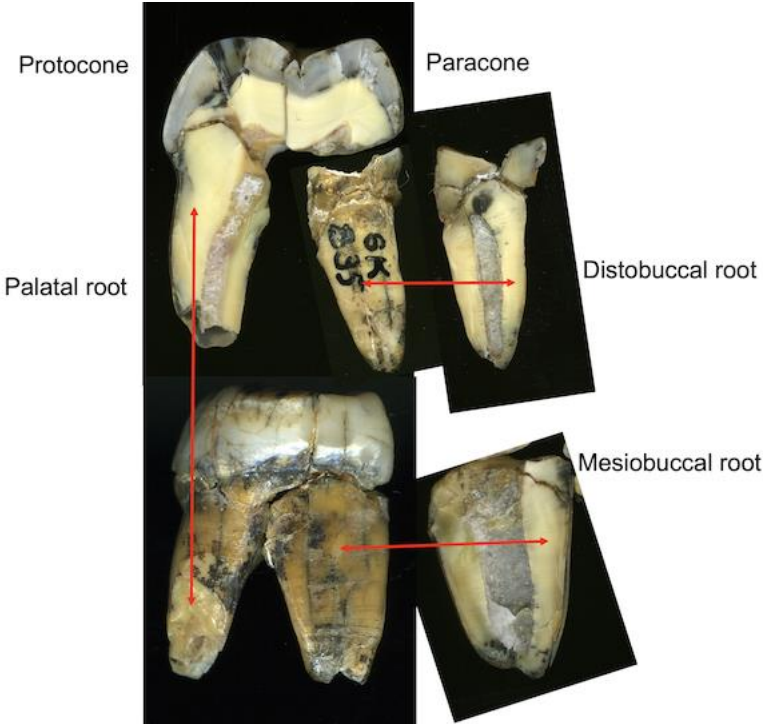
**Supplementary Figure S3.** Two *Gorilla* specimens as well as early *Homo* KNM-ER 820<sup>14,29</sup> and *A. africanus* drawing of specimen StW 151 (adapted from <sup>11</sup>) at stages close to M3 initiation.



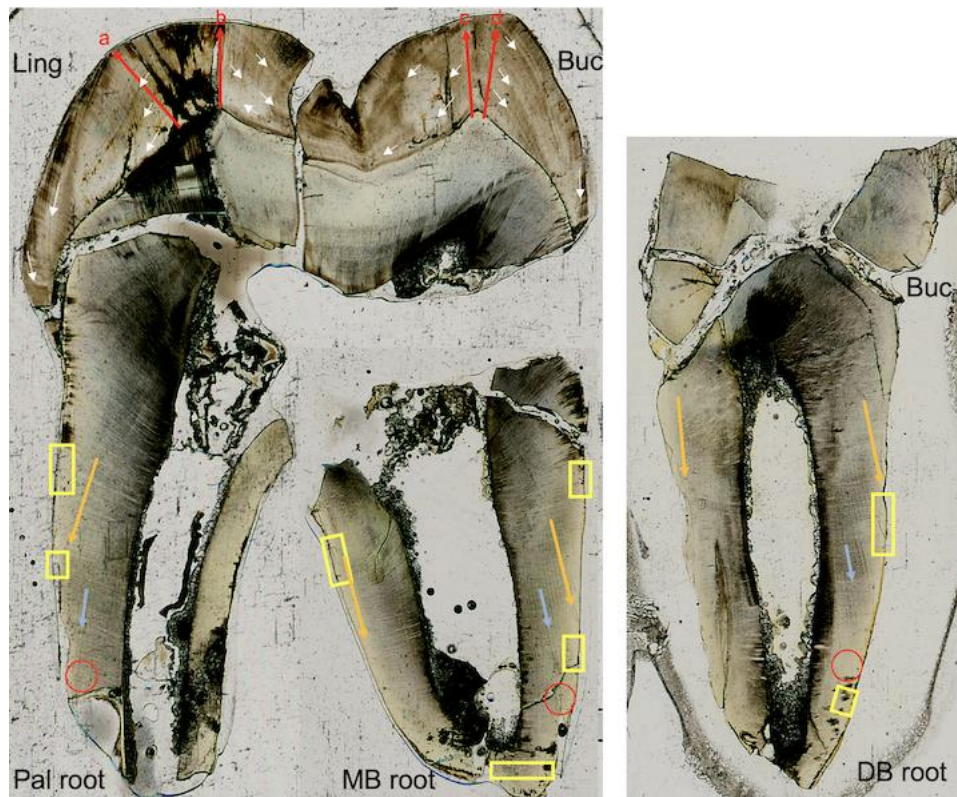
**Supplementary Figure S4.**  $\mu$ XCT-based 3D image of SK 835 with both the mesial dentine horns (arrows) in the plane of the histological section (line).



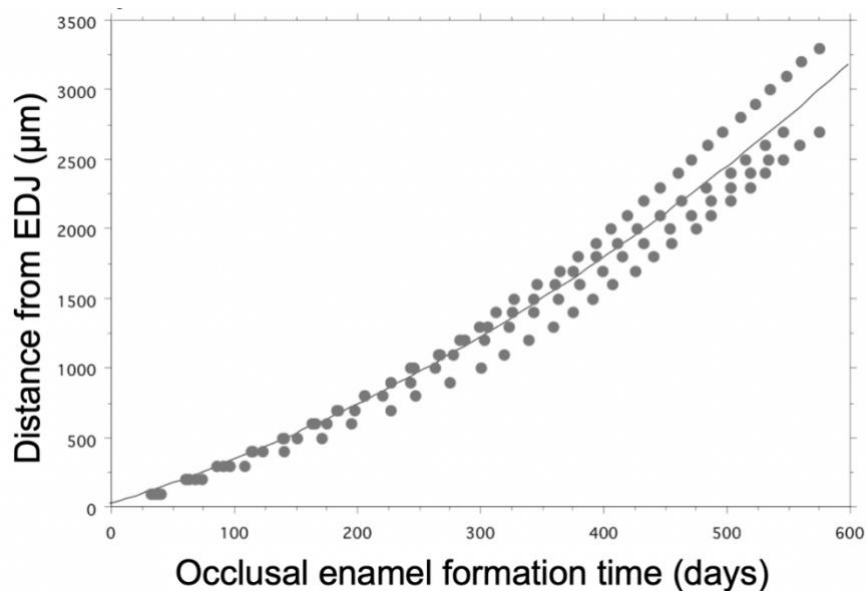
**Supplementary Figure S5.** SK 835: planes of section (in red) through the crown and roots.



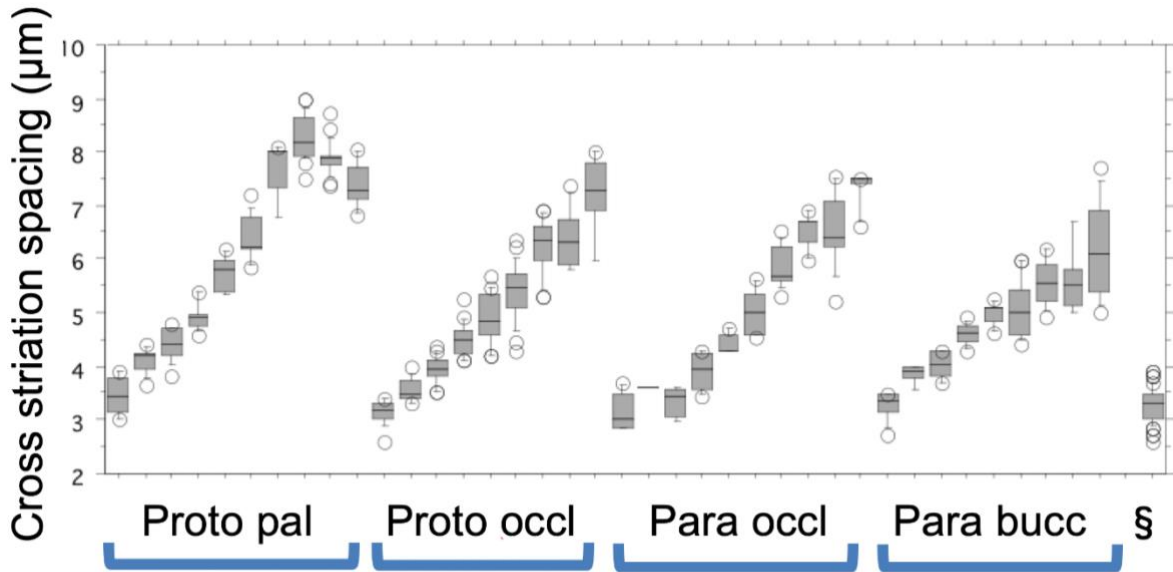
**Supplementary Figure S6.** SK 835: the polished block faces of the crown and roots aligned together.



**Supplementary Figure S7.** SK 835: three ground sections aligned together. Mesial section showing the palatal root to the very left beneath the protocone, and the mesio-buccal root to the right positioned beneath the paracone on the buccal aspect of the tooth. The disto-buccal root appears separately to the far right (See Supplementary Fig. S6). Matching accentuated lines in enamel (white arrows). Occlusal enamel trajectories ('a'-d' red arrows). Regions where daily dentine rates were identified and measured (yellow boxes). Position of prominent strontium lines in roots (orange arrows; see Sr map in Fig. 5). Matching accentuated lines in roots (blue arrows and red circles and at higher power in these regions in Supplementary Fig. S13). Buc: buccal; DB root: distobuccal root; Ling: lingual; MB root: mesiobuccal root; Pal root: palatal root.

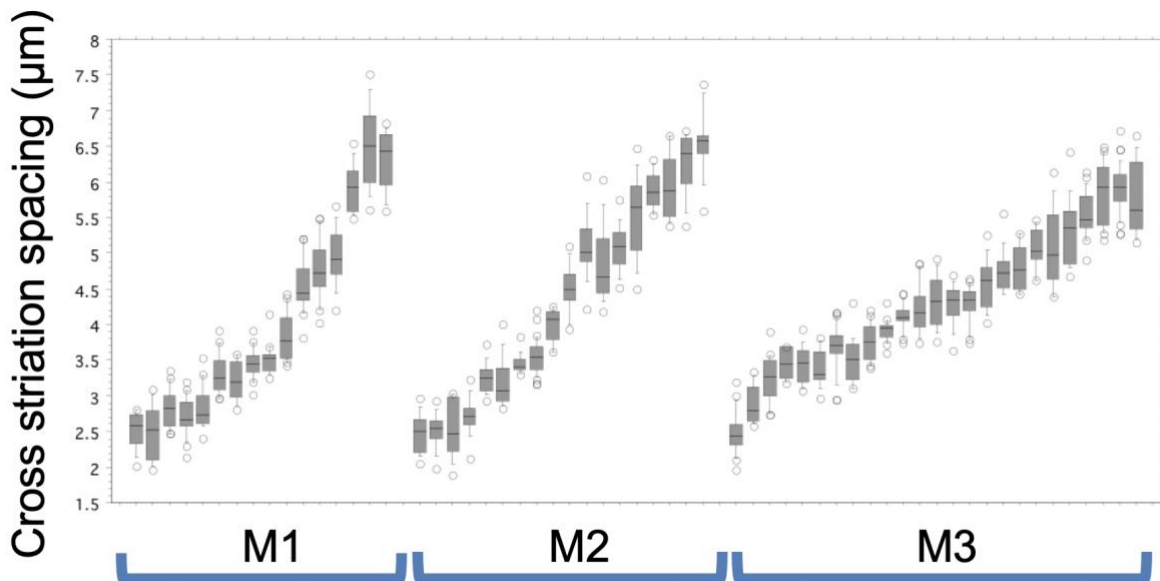


**Supplementary Figure S8.** SK 835: four occlusal trajectories (indicated by red arrows in Supplementary Fig. S7) with best fit line. Eq. 1:  $Y = 12.651 + .284X - 3.459e^{-5}X^2$  where Y is time in days.



### 60 day intervals of cuspal enamel formation in SK 835

**Supplementary Figure S9.** SK 835: gradients of increasing enamel formation rates at successive 60-day intervals along four occlusal tracks in the protocone and paracone as indicated in Supplementary Fig. S7 (red arrows ‘a’, ‘b’, ‘c’, ‘d’). ‘§’ represents all measurements made within 200 µm of the EDJ. The EDJ is to the left and the outer enamel surface to the right in all four cuspal plots.



### 30 day intervals of cuspal enamel formation

**Supplementary Figure S10.** Gradients of increasing occlusal enamel formation rates in three modern human molars from the same individual (30-day intervals). The EDJ is to the left and the outer enamel surface to the right in all three cuspal plots.

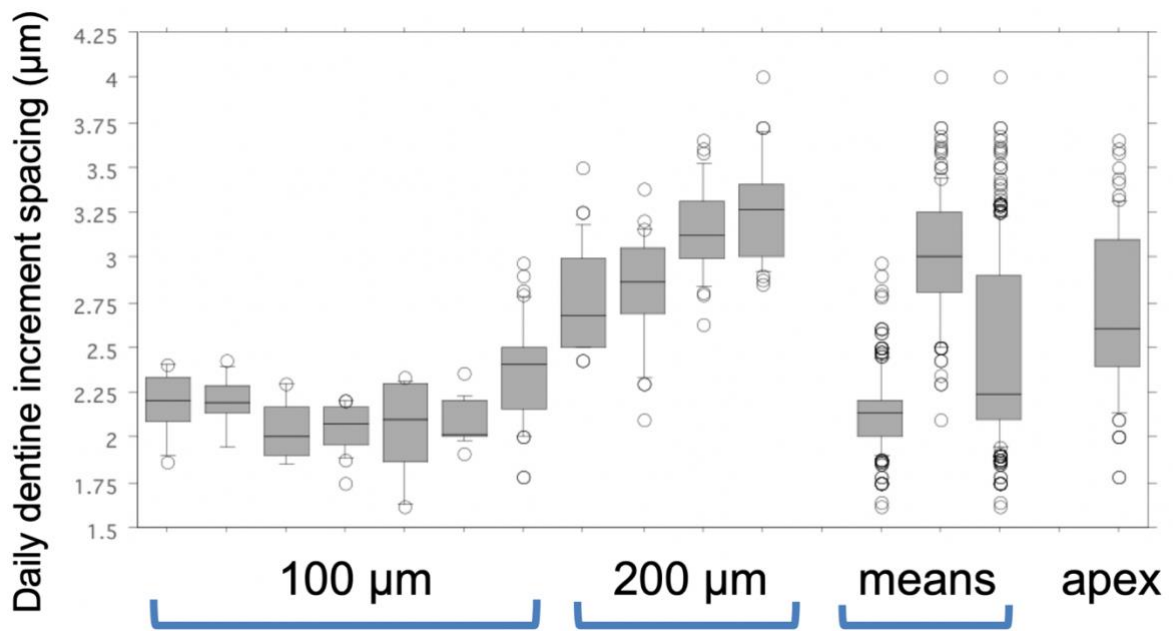
Protocone cervical enamel



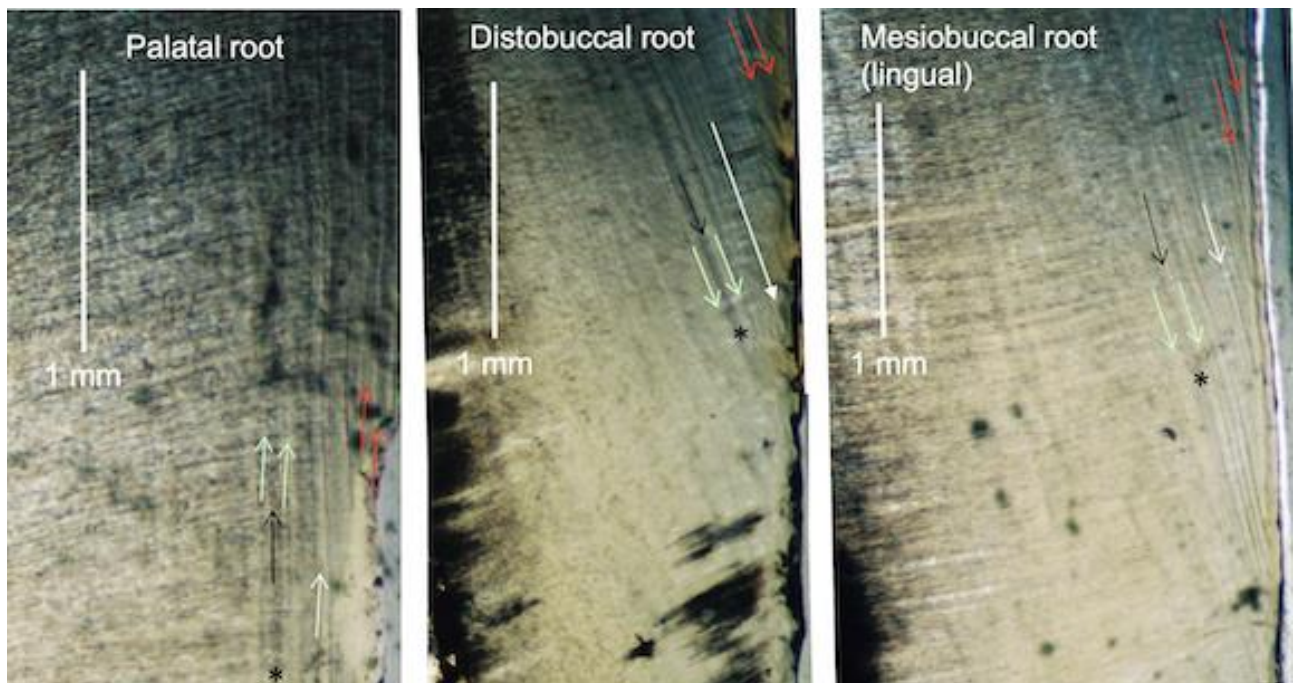
Paracone cervical enamel



**Supplementary Figure S11.SK 835:** daily cross striations and long-period incremental markings towards the cervical aspect of the lateral enamel (buccal paracone and palatal protocone). Apparently inconsistent periodicities, as well as indistinct regions where they were difficult to identify and count, excluded their use for any estimates of enamel formation times.

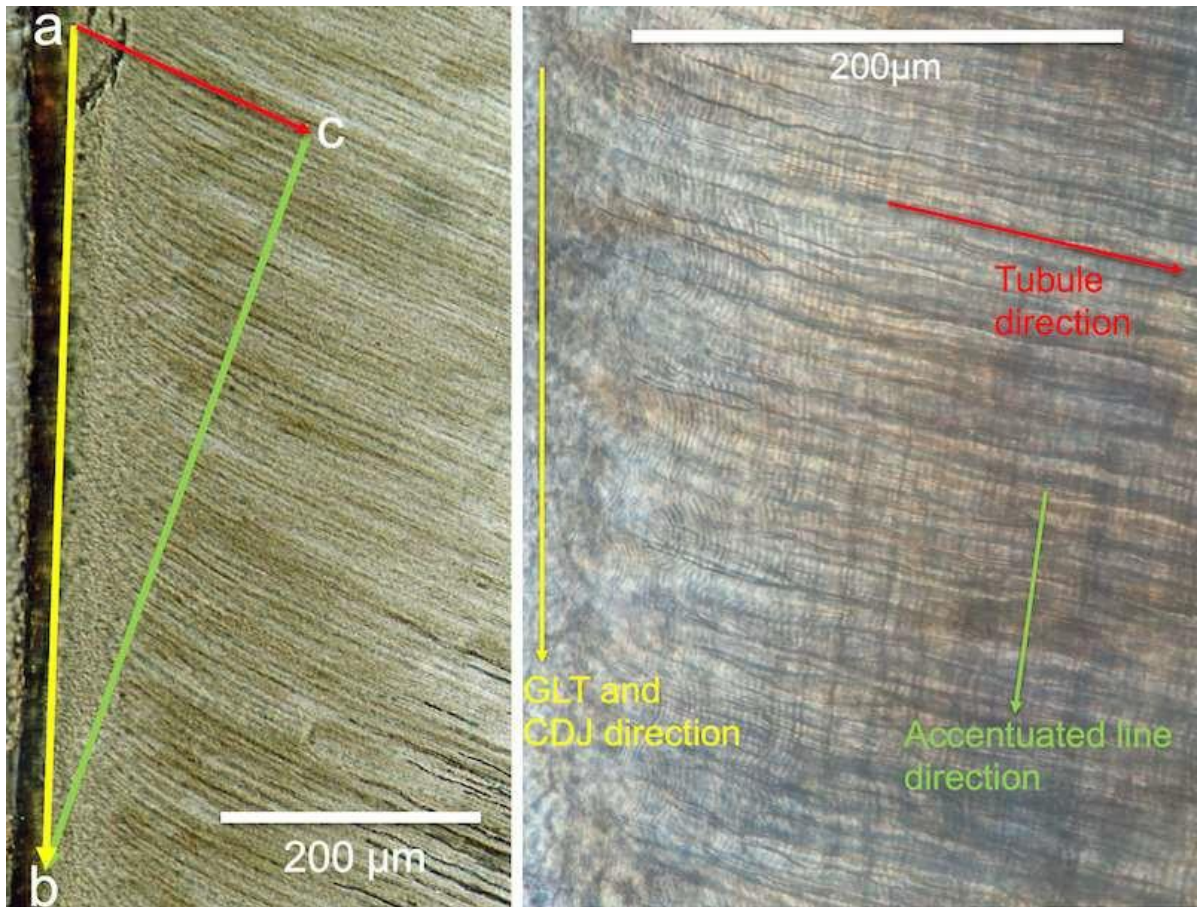


**Supplementary Figure S12.** SK 835: daily root dentine increment spacing ( $\mu\text{m}$ ) close to the CDJ with means for 100  $\mu\text{m}$ , 200  $\mu\text{m}$  and both zones averaged, as well as spacings measured in the apical root dentine (see Supplementary Fig. S7 for key).

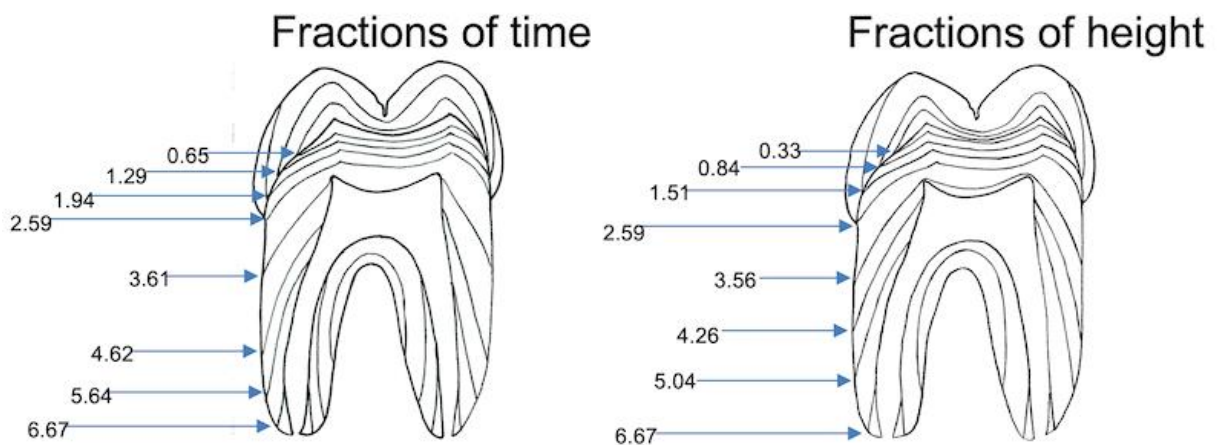


**Supplementary Figure S13.** SK 835: transmitted light micrographs of matching patterns of accentuated markings in root dentine. The red circles in Supplementary Fig. S7 indicate the locations of these examples.

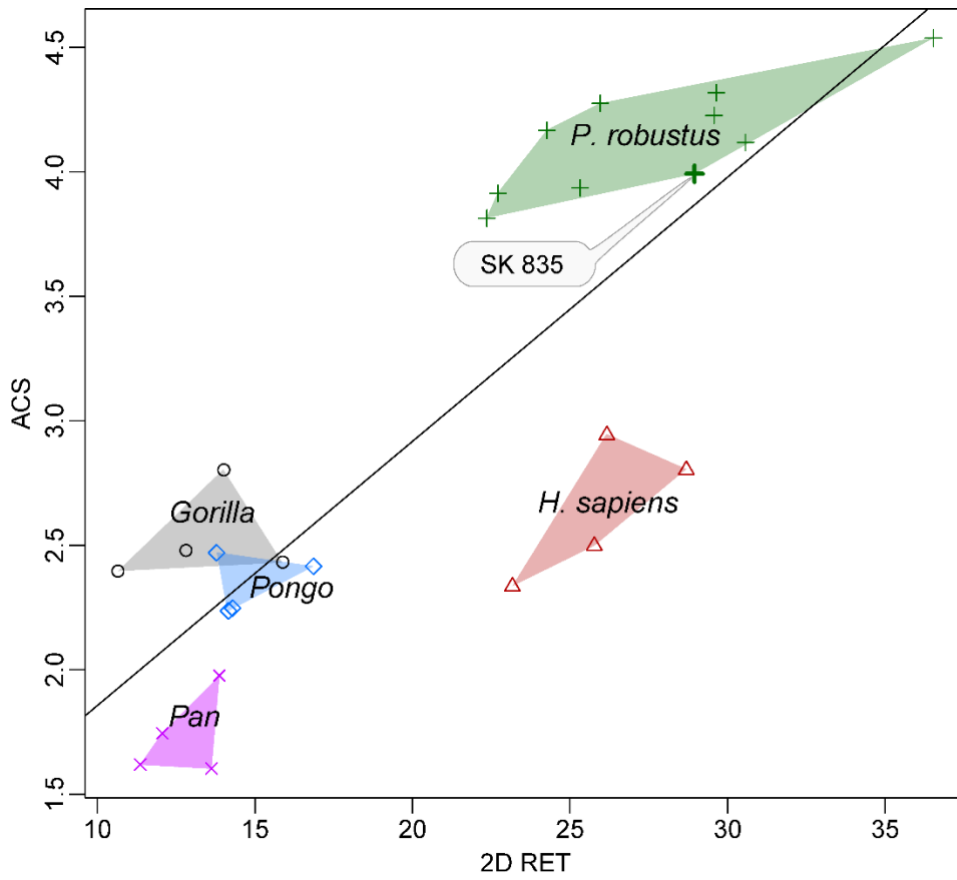




**Supplementary Figure S14.** SK 835. (left) The yellow arrow in root dentine runs just deep to cementum along the granular layer of Tomes (GLT) at the cementum dentine junction (CDJ), yellow arrow in both images, towards the root apex. The red arrow in both images runs in the direction of dentine tubules and the green arrow in both images runs in the direction of accentuated markings. The red line a-c is 200  $\mu\text{m}$  long. The time taken to form a-c (200  $\mu\text{m}$ ; average: 80 daily increments) also equals the time taken to extend between a-b (extension rate). (right) The annotated higher power image also shows each of these features but alongside daily root dentine increments and accentuated markings at higher resolution.



**Supplementary Figure S15.** Reconstructed M3 based on SK 835 showing incremental markings at  $\frac{1}{4}$  fractions of crown and root formation time and  $\frac{1}{4}$  fractions of crown and root height. Times of attainment (years) are arrowed along the EDJ and then along the CDJ.



**Supplementary Figure S16.** Bivariate plot of ACS against 2D RET in *P. robustus* (including SK 835) and extant hominid M3s with the regression line computed between the values for the two indices ( $Y = 0.795 + 0.106X$  where  $X$  is 2D RET;  $R^2=0.67$ ).

## Supplementary References

1. Liversidge, H. M. Timing of human mandibular third molar formation. *Ann. Hum. Biol.* **35**, 294–321 (2008).
2. Liversidge, H. M. Predicting mandibular third molar agenesis from second molar formation. *Acta Stomatol. Croat.* **42**, 311–317 (2008).
3. Beynon, A. D., Dean, M. C. & Reid, D. J. Histological study on the chronology of the developing dentition in gorilla and orangutan. *Am. J. Phys. Anthropol.* **86**, 189–203 (1991).
4. Dean, C. & Wood, B. A digital radiographic atlas of great apes skull and dentition. in *Digital Archives of Human Paleobiology, ADS Solutions* vol. 3 (L. Bondioli, R. Macchiarelli, Editors, 2003).
5. Schwartz, G. T., Reid, D. J., Dean, M. C. & Zihlman, A. L. A Faithful Record of Stressful Life Events Recorded in the Dental Developmental Record of a Juvenile Gorilla. *Int. J. Primatol.* **27**, 1201–1219 (2006).
6. Kuykendall, K. L. Dental development in chimpanzees (*Pan troglodytes*): The timing of tooth calcification stages. *Am. J. Phys. Anthropol.* **99**, 135–157 (1996).
7. Anemone, R. L., Mooney, M. P. & Siegel, M. I. Longitudinal study of dental development in chimpanzees of known chronological age: Implications for understanding the age at death of Plio-Pleistocene hominids. *Am. J. Phys. Anthropol.* **99**, 119–133 (1996).
8. Kralick, A. E. *et al.* A radiographic study of permanent molar development in wild Virunga mountain gorillas of known chronological age from Rwanda. *Am. J. Phys. Anthropol.* **163**, 129–147 (2017).
9. Reid, D. J. & Guatelli-Steinberg, D. Updating histological data on crown initiation and crown completion ages in southern Africans. *Am. J. Phys. Anthropol.* **162**, 817–829 (2017).
10. Dean, M. C., Beynon, A. D., Thackeray, J. F. & Macho, G. A. Histological reconstruction of dental development and age at death of a juvenile *Paranthropus robustus* specimen, SK 63, from Swartkrans, South Africa. *Am. J. Phys. Anthropol.* **91**, 401–419 (1993).
11. Moggi-Cecchi, J., Tobias, P. V. & Beynon, A. D. The mixed dentition and associated skull fragments of a juvenile fossil hominid from Sterkfontein, South Africa. *Am. J. Phys. Anthropol.* **106**, 425–465 (1998).
12. Le Cabec, A., Tang, N. K. & Tafforeau, P. Accessing developmental information of fossil hominin teeth using new synchrotron microtomography-based visualization techniques of dental surfaces and interfaces. *PLoS One* **10**, e0123019 (2015).
13. Smith, T. M. *et al.* Dental Ontogeny in Pliocene and Early Pleistocene Hominins. *PLoS One* **10**, e0118118 (2015).
14. Dean, M. C. The dental developmental status of six East African juvenile fossil hominids. *J. Hum. Evol.* **16**, 197–213 (1987).
15. Beynon, A. D. & Dean, M. C. Distinct dental development patterns in early fossil hominids. *Nature* **335**, 509–514 (1988).
16. Dean, M. C. A histological method that can be used to estimate the time taken to form the crown of a permanent tooth. in *Forensic Microscopy for Skeletal Tissues: Methods and Protocols* (ed. Bell, L. S.) vol. 915 89–100 (Humana Press, Springer Science and Business Media, 2012).

17. Guatelli-Steinberg, D., Floyd, B. A., Dean, M. C. & Reid, D. J. Enamel extension rate patterns in modern human teeth: Two approaches designed to establish an integrated comparative context for fossil primates. *J. Hum. Evol.* **63**, 475–486 (2012).
18. Dean, M. C. & Cole, T. J. Human Life History Evolution Explains Dissociation between the Timing of Tooth Eruption and Peak Rates of Root Growth. *PLoS One* **8**, e54534 (2013).
19. Dean, M. C., Humphrey, L., Groom, A. & Hassett, B. Variation in the timing of enamel formation in modern human deciduous canines. *Arch. Oral Biol.* **114**, 104719 (2020).
20. Boyde, A. Estimation of age at death of young human skeletal remains from incremental lines in the dental enamel. *Excerpta Medica Int. Congr. Ser.* **80**, 36–46 (1963).
21. Boyde, A. Developmental interpretations of dental microstructure. *Primate Life Hist. Evol. Monogr. Primatol.* **14**, 229–267 (1990).
22. Risnes, S. Enamel apposition rate and the prism periodicity in human teeth. *Eur. J. Oral Sci.* **94**, 394–404 (1986).
23. Antoine, D., Hillson, S. & Dean, M. C. The developmental clock of dental enamel: a test for the periodicity of prism cross-striations in modern humans and an evaluation of the most likely sources of error in histological studies of this kind. *J. Anat.* **214**, 45–55 (2009).
24. Shellis, R. P. Variations in growth of the enamel crown in human teeth and a possible relationship between growth and enamel structure. *Arch. Oral Biol.* **29**, 697–705 (1984).
25. Martin, L. Significance of enamel thickness in hominoid evolution. *Nature* **314**, 260–263 (1985).
26. Schwartz, G. T., McGrosky, A. & Strait, D. S. Fracture mechanics, enamel thickness and the evolution of molar form in hominins. *Biol. Lett.* **16**, 20190671 (2020).
27. Morphosource Database <http://www.morphosource.org> (2020).
28. Leakey, R. E. F. & Wood, B. A. New evidence of the genus *Homo* from East Rudolf, Kenya. II. *Am. J. Phys. Anthropol.* **39**, 355–368 (1973).
29. Wood, B. A. *Koobi Fora research project. Clarendon.* vol. Volume 4: Hominid cranial remains. (Clarendon Press, 1991).
30. Skinner, M. F. & Sperber, G. H. *Atlas of Radiographs of Early Man.* (Alan R. Liss, 1982).
31. Berger, L. R. *et al.* *Australopithecus sediba*: A new species of *Homo*-like australopith from South Africa. *Science* **328**, 195–204 (2010).
32. Le Cabec, A., Tafforeau, P., Smith, T. M., Carlson, K. J. & Berger, L. R. Dental Development of the *Australopithecus sediba* Juvenile MH1 Determined from Synchrotron Virtual Paleohistology. in *Proceedings of the European Society for the study of Human Evolution 3* 103 (2014).
33. ESRF. *Australopithecus Sediba at the ESRF.* (2010).
34. Leakey, R. E. F. & Walker, A. New *Australopithecus boisei* specimens from east and west Lake Turkana, Kenya. *Am. J. Phys. Anthropol.* **76**, 1–24 (1988).
35. Leakey, M. G. *et al.* New fossils from Koobi Fora in northern Kenya confirm taxonomic diversity in early *Homo*. *Nature* **488**, 201–204 (2012).
36. Brown, F., Harris, J., Leakey, R. & Walker, A. Early *Homo erectus* skeleton from west Lake Turkana, Kenya. *Nature* **316**, 788–792 (1985).
37. Kimbel, W. H. & Deleuzene, L. K. “Lucy” redux: A review of research on *Australopithecus*

- afarensis*. *Am. J. Phys. Anthropol.* **140**, 2–48 (2009).
38. Moggi-Cecchi, J., Menter, C., Boccone, S. & Keyser, A. Early hominin dental remains from the Plio-Pleistocene site of Drimolen, South Africa. *J. Hum. Evol.* **58**, 374–405 (2010).
  39. Tobias, P. *Olduvai Gorge, volume 4: The skulls, endocasts and teeth of Homo habilis*. (Cambridge University Press, 1991).
  40. Lordkipanidze, D. *et al.* Postcranial evidence from early *Homo* from Dmanisi, Georgia. *Nature* **449**, 305–310 (2007).
  41. Vekua, A. *et al.* A New Skull of Early *Homo* from Dmanisi, Georgia. *Science* **297**, 85 (2002).
  42. Cazenave, M. *et al.* Reassessment of the TM 1517 odonto-postcranial assemblage from Kromdraai B, South Africa, and the maturational pattern of *Paranthropus robustus*. *Am. J. Phys. Anthropol.* **172**, 714–722 (2020).
  43. Tobias, P. V. *The cranium and maxillary dentition of Australopithecus (Zinjanthropus) boisei*. vol. Olduvai Gorge. Vol. II (Cambridge University Press, 1967).
  44. Carney, J., Hill, A., Miller, J. A. & Walker, A. Late Australopithecine from Baringo District, Kenya. *Nature* **230**, 509–514 (1971).
  45. Schwartz, J. H. & Tattersall, I. *The Human Fossil Record. Craniodental Morphology of Genus Homo (Africa and Asia)*. vol. 2 (John Wiley & Sons, 2003).
  46. Zanolli, C. *et al.* Evidence for increased hominid diversity in the Early-Middle Pleistocene of Java, Indonesia. *Nat. Ecol. Evol.* (2019) doi:10.1038/s41559-019-0860-z.